

# Validation of an FE model updating procedure for damage assessment using a modular laboratory experiment with a reversible damage mechanism

Marlene Wolniak\*, Benedikt Hofmeister, Clemens Jonscher, Matthias Fankhänel, Ansgar Loose, Clemens Hübler, Raimund Rolfes

*Leibniz University Hannover / ForWind, Institute of Structural Analysis, Appelstr. 9A, 30167 Hannover, Germany*

---

## Abstract

In this work, the systematic validation of a deterministic finite element (FE) model updating procedure for damage assessment is presented using a self-developed modular laboratory experiment. A fundamental, systematic validation of damage assessment methods is rarely conducted and in many experimental investigations, only one type of defect is introduced at only one position. Often, the damage inserted is irreversible and inspections are only performed visually. Thus, the damage introduced and, with it, the results of the damage assessment method considered are often not entirely analyzed in terms of quantity and quality. To address this shortcoming, a modular steel cantilever beam is designed with nine reversible damage positions and the option to insert different damage scenarios in a controlled manner. The measurement data is made available in open-access form which enables a systematic experimental validation of damage assessment methods.

In order to demonstrate such a systematic validation using the modular laboratory experiment, a deterministic FE model updating procedure is applied, which was previously introduced by the authors. The results show a precise localization within  $\pm 0.05$  m of the nine different damage positions and a correct relative quantification of the three different damage scenarios considered. With that, this work demonstrates that the opportunity to introduce several reversible damage positions and distinctly defined types and severities of damage into the laboratory experiment presented enables the systematic experimental validation of damage assessment methods.

*Keywords:* Experimental validation, FE model updating, damage assessment, numerical optimization, modal analysis

---

## 1. Introduction

Monitoring engineering structures has become a vital part of civil engineering [1, 2] and a variety of different methods are applied in structural health monitoring (SHM) [3, 4, 5, 6]. The goal of monitoring is the identification of damage, which Worden et al. [7] defined as changes to the material, geometric properties, or both of these. Thus, in order to identify damage, the changes in the structural properties have to be identified by comparing at least two different states of the structure considered. Rytter [8] determined four categories which describe the level of damage identification: detection, localization, assessment (i.e., quantification) and consequence (i.e., remaining life-time prediction). Evidently, these levels increase in difficulty and each subsequent level requires the results of the previous one. The focus of this contribution is the introduction of a modular laboratory experiment with reversible damage mechanisms for the validation of SHM procedures addressing the third level – damage assessment, including the detection, localization and quantification of damage.

In order to examine and validate SHM methods, numerous experimental studies and real-life testing have been conducted over the years. Doebling et al. [9] give a comprehensive overview of applications of damage identification methods organized according to the type of structure. Examining the various experimental studies, it is noticeable that a great number of the implemented damage scenarios induce material degradation by the application of static loads (cf. e.g., [10, 11]) or by the introduction of saw cuts or kerfs (cf. e.g., [12, 13, 14]) into the structure under consideration. These damage mechanisms are irreversible in nature. Hence, usually only one fixed geometric damage location is analyzed in most experiments. However, the damage can be gradually increased in severity, so that different damaged states can be realized at the otherwise predetermined location(s). Regarding the inspection and thus the quantifiability of these common damage scenarios, a kerf can be sawn

---

\*Corresponding author

*Email address:* m.wolniak@isd.uni-hannover.de (Marlene Wolniak)

21 and measured precisely, whereas the progress of fatigue or creep damage due to loading is difficult to assess.  
22 Often, the inspections are only performed visually and the results obtained by the various SHM methods are  
23 typically only evaluated regarding the location of the defect inserted, and not its size or shape. The analysis of  
24 SHM applications to real-life structures in operation (cf. e.g., [1, 15, 16]) is limited, because there is normally  
25 no deliberate, precise defect insertion allowed. If damage is present in a particular structure, it is difficult to  
26 inspect thoroughly enough to determine the size and shape of the defects. Again, the results are typically only  
27 evaluated in terms of damage localization. Additionally, it is not always given that measurement data from  
28 operating structures are available in states before and after the damage event occurred, or there is no clear  
29 distinction between these states possible because the damage has occurred gradually.

30 In conclusion, although SHM methods have been validated in various experimental studies and real-life  
31 testing on operating structures, many of these application examples do not provide the opportunity for a  
32 thorough analysis and evaluation of the SHM methods considered. Especially in terms of the third level of  
33 damage identification, including damage detection, localization and quantification, comprehensive studies are  
34 still missing. With regard to the comparability of different SHM methods, another impairment of many of the  
35 publications examined is that they do not make the data from their application examples available. Thus, only  
36 the described results of the particular SHM method considered are published, leaving no opportunity for a fair  
37 comparison of different methods.

38 Of course, some benchmark problems with open-access raw data in the area of SHM already exist, which  
39 provide data for the comparison and analysis of different SHM methods. Prominent laboratory benchmark  
40 problems are the three-story building at the Los Alamos National Laboratory (LANL) [17, 18] or the four-  
41 story steel frame at the University of British Columbia (UBC) [19, 20]. Widely used benchmark problems  
42 involving full-scale engineering structures under environmental and operational conditions (EOCs) are the Z24  
43 bridge in Switzerland [21, 22], the rotor blade of the Vestas V27 wind turbine at the Technical University  
44 of Denmark [23, 24, 25] and the recently introduced lattice mast structure LUMO at the Leibniz University  
45 Hanover [26, 27]. However, these benchmark problems represent rather complicated application examples and  
46 are not always suitable when a basic, systematic validation of different SHM methods is sought to be performed.

47 All in all, the available benchmark problems provide the possibility for a validation and a comparison of dif-  
48 ferent SHM methods. However, they are characterized by rather difficult boundary conditions that complicate  
49 a basic validation of different damage assessment methods. This leads to the focus of this contribution, which is  
50 the presentation of a modular laboratory steel cantilever beam designed to facilitate a fundamental, systematic  
51 experimental validation of damage assessment methods in an entirely controlled setup. The modular experiment  
52 is conceptualized with several reversible damage positions and the option to insert different, accurately defined  
53 damage scenarios. The motivation for the design of the steel cantilever beam presented was to create a rather  
54 simple experiment, in which the structural behavior is entirely comprehensible and different SHM methods can  
55 be evaluated and compared at a fundamental level. In addition to the detailed description of the proposed  
56 experimental setup, the measurement data is made available in open-access form (see Data Availability State-  
57 ment) to ensure the opportunity for comparison. To demonstrate the application of the laboratory structure  
58 presented, an example systematic experimental validation of an FE model updating procedure addressing the  
59 third level of damage identification is outlined. Thereby, a detailed motivation and description of the FE model  
60 updating scheme utilized is presented.

61 This paper consists of six sections. Section 2 gives a detailed description of the experimental setup and the  
62 derived FE model used for the model updating procedure. Following this, the modal analysis technique utilized  
63 and an analysis of the modal data extracted from the measurements is described in Section 3. In addition,  
64 a comparison of the dynamic properties of the initial FE model against the extracted modal data from the  
65 measurements is highlighted. FE model updating is further introduced in Section 4 and the herein considered  
66 deterministic FE model updating procedure and the optimization scheme utilized are described in detail. The  
67 results are displayed, analyzed and discussed in Section 5. Finally, Section 6 gives a summary and an outlook.

## 68 2. Experimental setup

69 The steel cantilever beam considered is a modular setup of a central beam structure with nine screwed-on  
70 fishplates. The fishplates are used to implement a variable, reversible damage mechanism. A schematic overview  
71 and a photograph of the modular beam structure are given in Figures 1 and 2.

72 The central beam and the screw-on fishplates are fabricated from rectangular stainless-steel bar stock. As  
73 depicted in Figure 1 and visible in Figure 2, the fishplates are screwed on in alternating positions above and  
74 below the central beam structure with an overlap of 10 mm. The M5 screws utilized have a uniform separation of  
75 20 mm, yielding a total of sixty screws to connect the fishplates to the center line of the central beam. Thus, each

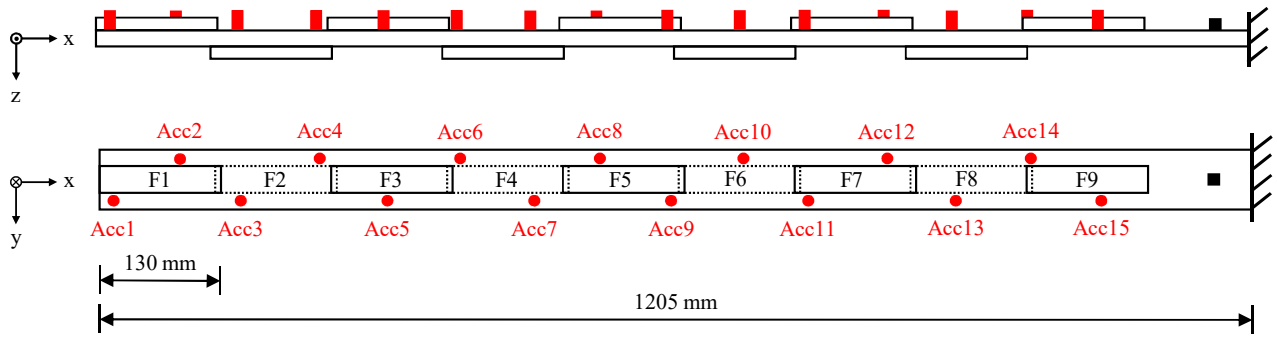


Figure 1: Schematic overview of the steel cantilever beam.

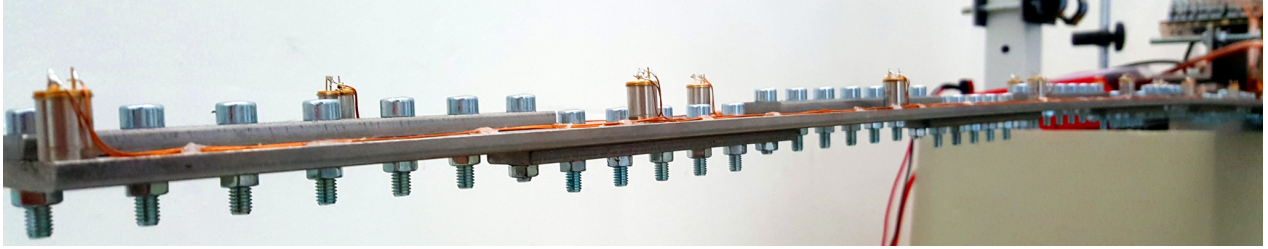


Figure 2: Photograph of the steel cantilever beam.

76 fishplate is held in place by seven screws, whereby the overlapping fishplates share one screw at each respective  
 77 end. To ensure a repeatable fishplate connection stiffness, the screws are tightened with a consistent assembly  
 78 torque of 5 Nm. The fishplates and screw connections are dimensioned to yield contact pressure sufficient to  
 79 suppress shear movement between the central beam structure and the fishplates by friction. The dimensions of  
 80 the central beam and the fishplates are listed in Table 1. In addition, a close-up of the tip of the steel cantilever  
 81 beam is shown in Figure 3, where the accelerometers, wiring and M5 screws are visible.

Table 1: Dimensions of the central beam structure and the screwed-on fishplates.

	Dimension	Value in mm
Central beam	Length	1205
	Width	60
	Thickness	5.15
Fishplates	Length	130
	Width	20
	Thickness	4.85

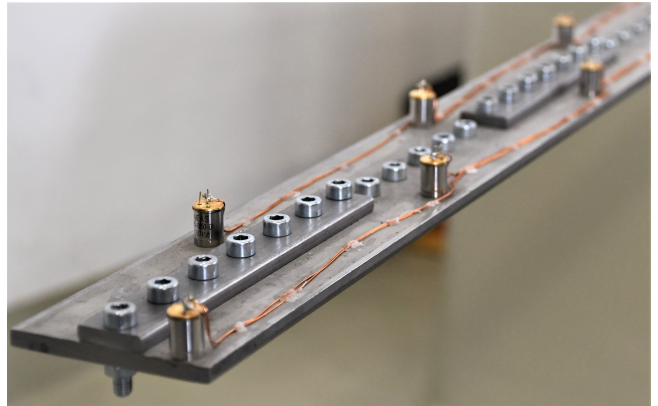


Figure 3: Close-up of the tip of the steel cantilever beam.

82 The central beam with nine undamaged screw-on fishplates represents the reference state of the considered  
 83 experiment. The reversible damage mechanism is activated by swapping the intact fishplates with damaged  
 84 fishplate specimens (see Section 2.2 for photographs of the damaged fishplate specimens). Since the fishplates  
 85 are fixed using screws, the mechanism can be activated and deactivated without causing permanent alterations  
 86 to the structure or the fishplates. As a result, the particular experimental setup with a reversible damage  
 87 mechanism and different variable damage positions allows for the consideration of a variety of damage scenarios.

### 88 2.1. Sensors, measurement system and type of excitation

89 As the experimental structure is relatively small and light, the sensors are chosen accordingly. A total of  
 90 fifteen miniature IEPE accelerometers with a dynamic range of  $\pm 500 \frac{m}{s^2}$  are connected to the central beam

91 structure. The sensors weigh only 5 g each and are attached along the steel beam with a uniform separation of  
 92 80 mm using integrated M3 screw connectors. The placement alternates between the right and left side of the  
 93 beam, as indicated in Figure 1. This way, also torsional mode shapes can be identified. The accelerometers are  
 94 connected to the measurement system using enameled copper wires, leaving from the sensors as demonstrated  
 95 in the close-up view shown in Figure 3. A terminal block next to the fixed end of the beam is used to connect  
 96 the enameled copper wires to the measurement lines. The sensors are powered using IEPE current supplies,  
 97 which are connected to a 24-bit measurement system. Thereby, the use of IEPE sensors ensures rejection of  
 98 grid hum and a high signal-to-noise ratio [28]. The sampling frequency of the measurement system was set to  
 99 1200 Hz.

100 The steel cantilever beam is excited using a proprietary, contact-free electromagnetic shaker placed at the  
 101 root of the beam (black square in Figure 1). All measurements were conducted with broadband white-noise  
 102 excitation up to 250 Hz using a signal-generating computer and a digital-to-analogue converter connected to  
 103 a power amplifier. Utilizing broadband white noise ensures the excitation of all eigenmodes in the chosen  
 104 frequency range.

## 105 2.2. Damage scenarios and experimental procedure

106 For the representation of realistic damage scenarios, structural damage is assumed to manifest itself as  
 107 stiffness deviations in a certain geometric area of a structure. In the laboratory experiment conducted, damage  
 108 is introduced by sawing cuts into a fishplate specimen. This locally weakens the cross-section of the fishplate.  
 109 In this work, three different damage scenarios are considered, subsequently named as "discrete", "Gaussian  
 110 distributed" and "uniformly distributed" damage. Figure 4 shows a photograph of each damaged fishplate.



Figure 4: Photographs of the three differently damaged fishplates.

111 The damaged fishplates are designed to have the same weight of 91 g as the undamaged fishplates. Since each  
 112 saw cut has a width of approximately 1 mm, some material is removed. To compensate for this, the damaged  
 113 fishplates are fractions of a millimeter wider than the undamaged ones. This is necessary to guarantee that the  
 114 changes introduced in the structural dynamic behaviour are only due to stiffness variations and not due to mass  
 115 differences.

116 The experimental procedure comprises three measurement series - one series for each damage scenario (i.e.,  
 117 discrete, Gaussian and uniformly distributed). Each measurement series involves screwing the respective  
 118 damaged fishplate specimen onto all nine fishplate positions in sequence. In addition, before the measurement  
 119 of each damaged state of the cantilever beam, the reference state is restored and a measurement of this intact  
 120 state is conducted. Thus, every measurement series consists of  $9 \cdot 2 = 18$  measurements, with each measurement  
 121 comprising 1 hour of data. Table 2 gives an overview of the configuration of the experiments.

122 For the three measurement series conducted with 18 measurements of 1 hour each, this results in a total of 54  
 123 hours of measurement data. Hence, the experiment was conducted over several weeks, resulting in small changes  
 124 in the environmental conditions at the experimental site over this time period. Although the experiment was  
 125 performed in a laboratory, temperature changes and environmental influences like other machinery operating in  
 126 the laboratory or even small events like people passing the experiment, thus causing vibrations in the laboratory  
 127 floor, have an effect on the measurements. Additionally, several scientists were involved in the execution and

Table 2: Experimental procedure and measurement times.

Measurement series	Scenario	Fishplate position			
		1	2	...	9
1	Reference state	1 h	1 h		1 h
	Discrete damage	1 h	1 h		1 h
2	Reference state	1 h	1 h		1 h
	Gaussian distributed damage	1 h	1 h		1 h
3	Reference state	1 h	1 h		1 h
	Uniformly distributed damage	1 h	1 h		1 h

128 recording of the measurements, resulting in slight differences in the screw-on mounting of the fishplates or the  
129 adjustment of the shaker excitation. However, the measurement setup, the setup of the recording measurement  
130 system and the method of extraction of the modal data remained identical throughout the whole experiment.

131 In summary, as is the case for all practical experiments to a greater or lesser degree, there were some  
132 influences which affected the measurements that could not be excluded, even though great attention was given  
133 to achieving the same conditions for all measurements in all three measurement series. Nevertheless, these  
134 influences only caused marginal changes and uncertainties in the measurement and, as a result, in the extracted  
135 modal data.

136 The measurement data used in this work including a comprehensive documentation is uploaded to a public  
137 data repository of the Leibniz University Hanover and can be reached under the following link:  
138 <https://doi.org/10.25835/123gy6gm>.

### 139 2.3. Finite element model

140 The aim of the FE model updating procedure considered in this work is damage localization and quantifica-  
141 tion along the length of the steel cantilever beam. To fulfil this aim, a beam model is chosen as a representation of  
142 the steel cantilever beam, as it is sufficient for the task and computationally inexpensive. The later is important  
143 since the FE model updating procedure represents an optimization process, in which the computational costs  
144 of multiple evaluations of the underlying numerical model become an issue. With this rather small FE model  
145 incorporating few degrees of freedom, the modal analysis step takes only seconds. Thus, extensive numerical  
146 studies are made possible.

147 The varying sectional properties along the beam structure are assigned to the beam elements using general  
148 cross-sectional parameters. Three sections are defined for the fishplates positioned above and below the central  
149 beam and where two fishplates overlap (cf. Figure 1). The sectional properties assigned are listed in Table  
150 3. The material properties of stainless steel are utilized, and the omitted mass due to the screw holes and the  
151 additional mass of the sixty screws connecting the fishplates to the central beam are taken into account by  
152 adjusting the density of the standard material ( $7900 \frac{\text{kg}}{\text{m}^3}$ ). Given that the screw holes have an average diameter  
153 of 5 mm and the average mass of a screw and a nut is 5.1 g, the density is increased to a value of  $8500 \frac{\text{kg}}{\text{m}^3}$ . The  
154 weight of the enameled copper wiring is neglected as this is an insignificantly low weight relative to the bulk of  
155 the steel cantilever beam.

Table 3: Sectional properties assigned to the beam elements of the FE model.

Section	Description of fishplate position	Area in $\text{mm}^2$	$I_{11}$ in $\frac{\text{N}}{\text{mm}^2}$	$I_{22}$ in $\frac{\text{N}}{\text{mm}^2}$	J in $\frac{\text{N}}{\text{mm}^2}$	Offset center line in mm
1	Above central beam	406	2719	959	5504	1.2
2	Below central beam	406	2719	959	5504	-1.2
3	Overlap	503	5913	992	9526	0

156 The miniature accelerometers have a mass of 5 g each and are simulated as point masses at the corresponding  
157 locations along the beam (cf. Figure 1). The offset of the sensor positions is taken into account by placing  
158 additional nodes  $\pm 20$  mm orthogonally from the centre line of the beam, alternating to the left and right,  
159 and assigning the point masses to these offset nodes. A kinematic constraint couples the offset nodes to the  
160 corresponding nodes of the model. At the root of the steel cantilever beam, all degrees of freedom are set to  
161 zero, representing the fixed support.

162 The beam model represents the reference model of the intact steel cantilever beam and is used as the basis  
 163 for the following FE model updating procedure. The simulations are conducted using the FE analysis software  
 164 Abaqus.

### 165 3. Modal analysis

166 In order to ensure high-quality modal data as an input for the FE model updating procedure, an advanced  
 167 identification method is used for the extraction of modal data from the measurements.

#### 168 3.1. Identification method

169 The identification method chosen is based on the frequency domain decomposition (FDD) [29]. A singular  
 170 value decomposition is performed on the power spectral density (PSD) matrix  $G_{yy}$  of the structural responses

$$\mathbf{G}_{yy}(f_k) = \mathbf{U}_k \mathbf{S}_k \mathbf{U}_k^H, \quad (1)$$

171 where  $f_k$  is the frequency,  $\mathbf{U}_k$  is a unitary matrix of the singular vectors  $\mathbf{u}_{k_i}$  and  $\mathbf{S}_k$  is a diagonal matrix of the  
 172 singular values  $s_{k_i}$ . In the case of well-separated modes and white-noise excitation, only one mode dominates  
 173 in the vicinity of the natural frequency  $f_0$ . As a consequence, the largest singular value dominates close to an  
 174 eigenfrequency. Peak picking is used to determine the natural frequency and the eigenmode is identified from  
 175 the corresponding singular vector. The singular value curve in the vicinity of the mode corresponds to the  
 176 curve of a PSD of a single-degree-of-freedom (SDOF) oscillator [30]. Therefore, a more accurate identification  
 177 of the natural frequency is achieved by fitting the theoretical PSD  $h$  of an SDOF to the measured singular value  
 178 spectrum. For acceleration signals, the PSD is

$$h(f_0, \zeta, S, e, f_k) = \frac{(2\pi f_k)^4 S^2}{(4\zeta^2 - 2)\eta_k^2 + \eta_k^4 + 1} + e, \quad \eta_k = \frac{f_k}{f_0}, \quad (2)$$

179 where  $\zeta$  is the damping ratio,  $S$  is the modal force and  $e$  denotes the model error. The model error and the  
 180 modal force are assumed to be constant across the frequency range considered. The model error represents the  
 181 measurement noise and signal components which do not match the SDOF spectrum. The identification of the  
 182 four parameters is achieved using numerical optimization. The resulting least-squares problem is

$$\min \left( \sum_{k=k_l}^{k_u} (h(f_0, \zeta, S, e, f_k)^2 - s_{k_l}^2) \right), \quad (3)$$

183 where  $k_l$  and  $k_u$  are the indices of the lower and upper frequency limits of the range under consideration.

#### 184 3.2. Extracted modal data

185 Before a detailed overview of the extracted modal properties in both the reference state and the different  
 186 damaged states is given in the following two subsections, an insight into the identification settings used for  
 187 the extraction of the modal data is presented. As the attached accelerometers measure only in the vertical  
 188 direction, horizontal mode shapes are not recorded properly. Occuring torsional modes can be identified due to  
 189 the alternating placement of the accelerometers (cf. Section 2). Nevertheless, horizontal and torsional modes  
 190 are not sufficiently excited for a distinct identification using the FDD, because the excitation applied to the steel  
 191 cantilever beam exclusively operates in the vertical direction. Thus, only the modal properties corresponding to  
 192 pure vertical bending modes are included in the subsequent FE model updating procedure and all other modes  
 193 are neglected in this work. The alternating sensor positions were chosen anticipatory as subsequent applications  
 194 might include a differing excitation.

195 Table 4 lists the frequency ranges applied for the first four extracted eigenfrequencies related to pure vertical  
 196 bending mode shapes and in Table 5 other identification settings regarding, e.g., the sampling rate, measurement  
 197 time and window length are given. As the measurement time is chosen differently in the subsequent evaluations,  
 198 it is listed as a value  $t$ .

##### 199 3.2.1. Reference state and comparison to the finite element model

200 According to the design of the experiments outlined in Table 2, the reference state of the cantilever beam was  
 201 reconstituted and measured for a total of  $9 \cdot 3 = 27$  times, resulting in 27 hours of measurement data. As already  
 202 mentioned in Section 2, some environmental conditions and personal influences affected the measurement data.

Table 4: Frequency range used for the extraction of the modal data.

Eigenfrequency no.	$f_l$ in Hz	$f_u$ in Hz
1	3	5
2	22	25.5
3	60	80
4	195	235

Table 5: Identification settings used for the extraction of the modal data.

Setting	Assignment
Sampling rate	1200 Hz
Measurement time	$t$ in s
Window	Hanning
Window length	1200 Hz · $t$
Zero padding	0
Overlapping data points	0

203 This is why the extracted modal data from the 27 hours of measurement in the reference state show small  
 204 variance, which is presented and analyzed in the following.

205 Table 6 gives an overview of the statistical data of the four eigenfrequencies identified from all 1 h-measurements  
 206 in the reference state (i.e.,  $t = 3600$  s). Furthermore, the corresponding eigenfrequencies calculated with the  
 207 previously introduced FE model are listed together with their percentage deviation ( $\Delta f$ ) from the median value  
 208 of the respective eigenfrequency extracted from the measurements. Thereby, the corresponding eigenmodes are  
 209 selected by employing the well-known modal assurance criterion (MAC) defined by Allemang [31]. The MAC  
 210 determines the degree of similarity between two mode shape vectors, returning a value of one if the mode shapes  
 211 compared are linearly dependent, and a value of zero if they are linearly independent. Naturally, the allocation  
 212 of the simulated mode shapes to the measured ones is decided with respect to the highest MAC value. Figure  
 213 5 visualizes the MAC values of the vertical mode shape deflection at the fifteen sensor positions shared by the  
 214 four measured and the first ten simulated mode shapes in the reference state.

Table 6: Quartile values of the first five extracted eigenfrequencies from all 1 h-measurements in the reference state and a comparison to the corresponding modal properties calculated with the FE model.

Eigen-frequency no.	Measurement			FE model in Hz	Comparison	
	First quartile in Hz	Median in Hz	Third quartile in Hz		$\Delta f$ in %	MAC
1	3.931	3.934	3.940	3.90	-0.86	0.9989
2	24.478	24.503	24.516	24.44	-0.26	0.9984
3	68.251	68.353	68.406	68.43	0.11	0.9965
4	218.644	218.851	219.127	221.39	1.16	0.9848

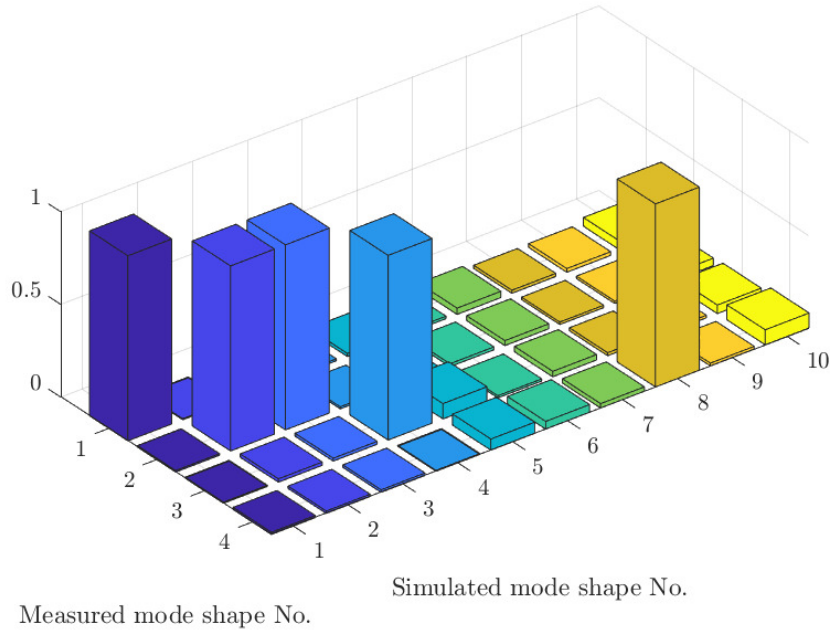


Figure 5: MAC values of the vertical mode shape deflection at the fifteen sensor positions shared by the measured and simulated mode shapes in the reference state.

215 As is evident from Figure 5, the matching of the simulated mode shapes to those extracted from the  
 216 measurements based on the MAC value alone gives a conclusive result for the first, third and fourth measured  
 217 mode shapes. The second measured mode shape shows a high correlation to both the second and third simulated  
 218 mode shapes. Here, a distinct selection can be reached by considering the deflection direction of the simulated  
 219 modes. As the second simulated mode shape has its main deflection amplitude in the horizontal direction,  
 220 this horizontal bending mode can be eliminated, despite showing a high MAC value with respect to the second  
 221 measured shape. The actual deflection shapes of the first four bending modes extracted from the measurements  
 222 in the reference state are shown in Figure 6. In conjunction with Table 6, Figure 6 depicts the 1 h-median  
 223 values of the normalized vertical deflection amplitude at the fifteen sensor positions. Furthermore, the values  
 224 of the normalized vertical deflection amplitude at the fifteen (simulated) sensor positions of the corresponding  
 225 simulated mode shapes are added. To support the visualization, the discrete values at the sensor positions are  
 226 connected by linear interpolation.



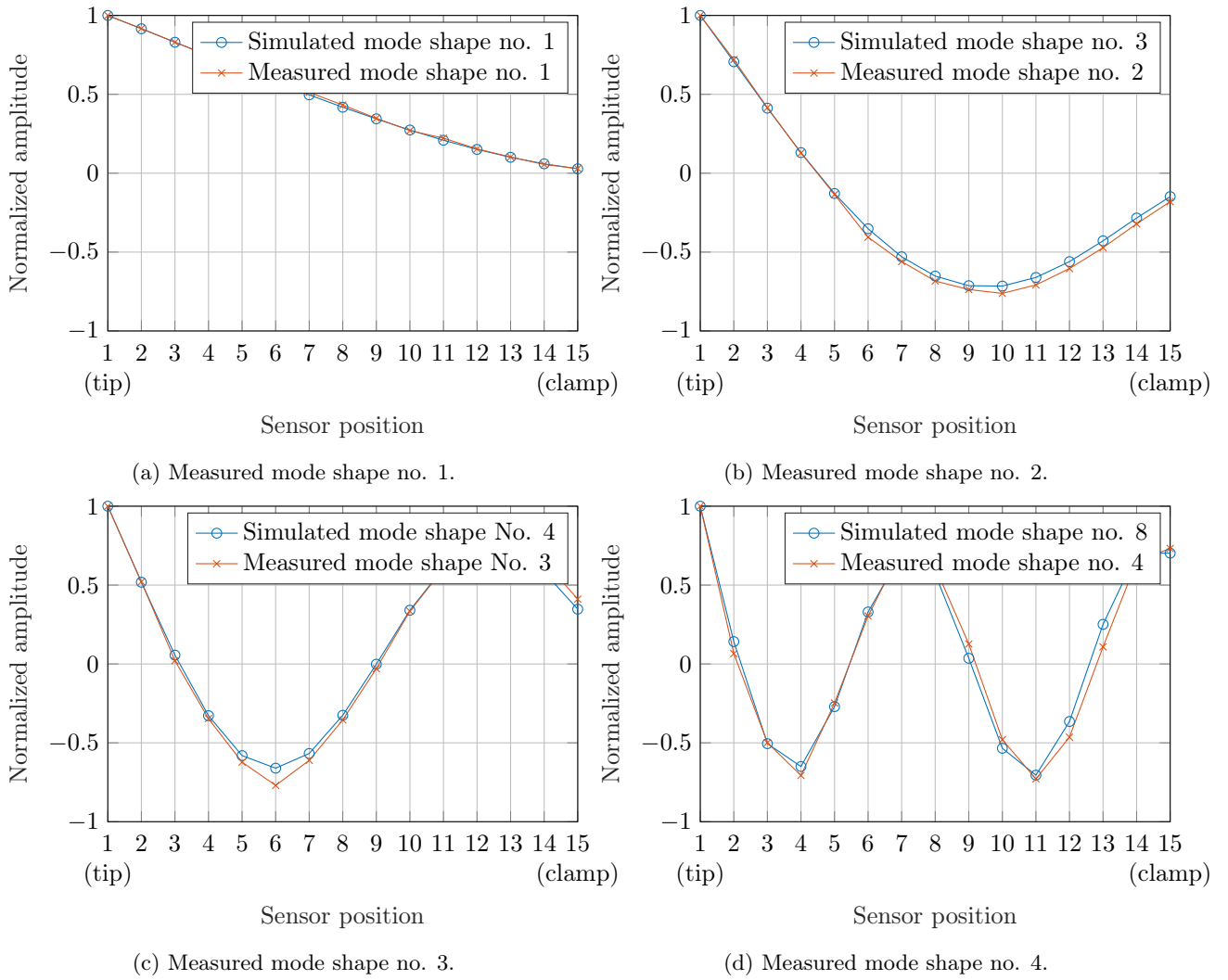


Figure 6: Comparison of the normalized vertical deflection amplitude of the first four bending modes extracted from all measurements in the reference state with the selected simulation results at the fifteen sensor positions.

227 *3.2.2. Damaged states*

228 The damaged states are obtained by swapping the intact fishplates with damaged fishplate specimens in  
 229 sequence. Thus, a total of 27 different damaged states were measured (cf. Table 2). Thereby, each geometric  
 230 position and each damage scenario influences the modal properties of the steel cantilever beam in a different  
 231 way.

232 In order to provide an overview of the effect of the different damaged states, the alteration of the first  
 233 and second eigenfrequency is considered in more detail. For an increase of the statistical evidence, all 1h-  
 234 measurements of the different damaged states are divided into six 10 min-data sets. Figures 7 and 8 show  
 235 the boxplots of the first and second eigenfrequency extracted from the discrete and the uniformly distributed  
 236 damage state, using the 10 min-data sets. To render the variations of the damaged states with respect to the  
 237 reference state, a solid line is added to indicate the median value and two dashed lines are added to indicate the  
 238 first and third quartile values of the corresponding eigenfrequencies extracted in the reference state (cf. Table  
 239 6).

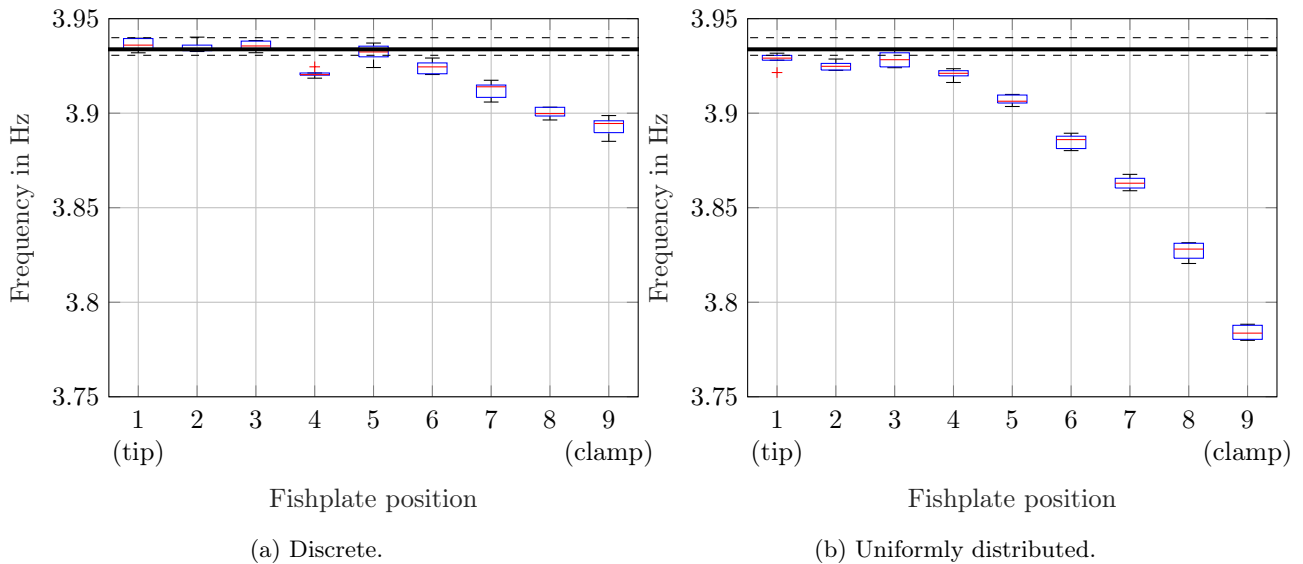


Figure 7: Boxplots of the first eigenfrequency extracted from the discrete and the uniformly distributed damage scenario. The solid line indicates the median value and the dashed lines indicate the first and third quartile values of the corresponding eigenfrequency in the reference state.

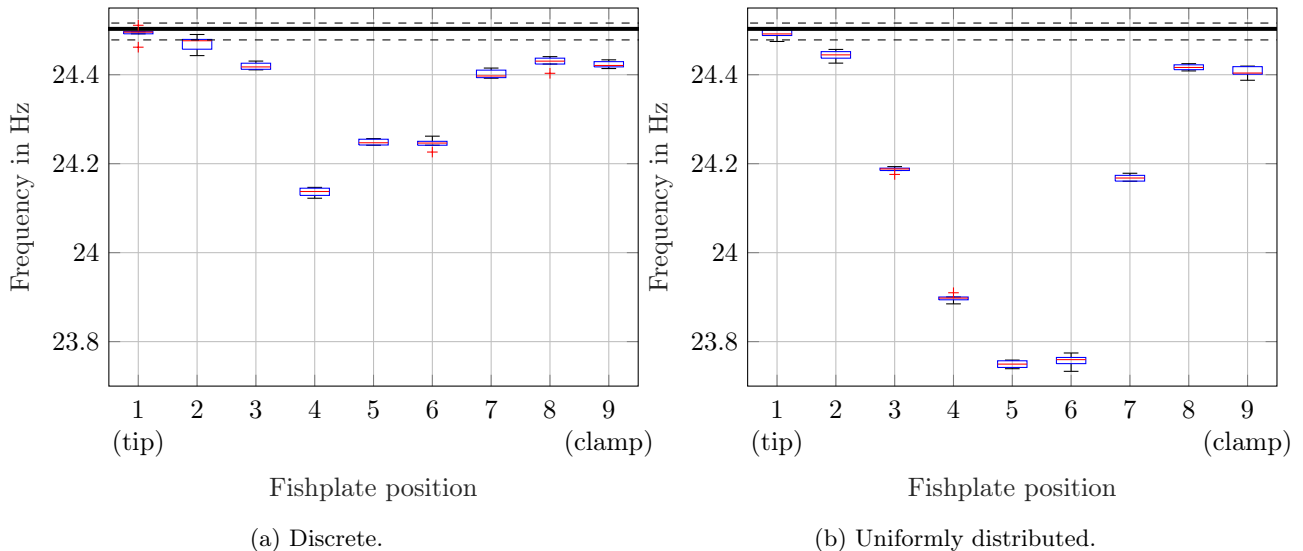


Figure 8: Boxplots of the second eigenfrequency extracted from the discrete and the uniformly distributed damage scenario. The solid line indicates the median value and the dashed lines indicate the first and third quartile values of the corresponding eigenfrequency in the reference state.

240 First of all, an observation of the eigenfrequency deviations in Figures 7 and 8 clearly reveals a stiffness  
 241 reduction of the beam caused by a screw-on of the damaged fishplate specimens: The eigenfrequencies extracted  
 242 from the damage scenarios are primarily lower than the median value of the corresponding eigenfrequencies  
 243 extracted in the reference state.

244 As the damage scenarios considered range from small to more severe stiffness alterations (cf. Figure 4), their  
 245 influence on the modal properties of the steel cantilever beam differ respectively. In the following, the intensity of  
 246 the influence of each damage scenario is examined using the example of the alteration of the first eigenfrequency  
 247 and the damaged fishplate position 9. Table 7 lists the median value of the first eigenfrequency extracted from  
 248 the 10 min-data sets of each damage scenario of fishplate position 9. In addition, the percentage deviation with  
 249 respect to the corresponding median value of 3.934 Hz is listed, calculated using all 27 1 h-measurements in the  
 250 reference state (cf. Table 6).

Table 7: Median values of the first eigenfrequency extracted from the 10 min-data sets of the three damage scenarios of fishplate position 9 and comparison with the respective median value of 3.934 Hz extracted from all measurements in the reference state.

Damage scenario	Median in Hz	$\Delta f$ in %
Discrete	3.895	-0.99
Gaussian distributed	3.877	-1.45
Uniformly distributed	3.784	-3.81

Table 7 clearly demonstrates that the increasing severity of the three damage scenarios is reflected in the intensity of the eigenfrequency deviation. Whereas the deviation caused by the Gaussian distributed damage only slightly increases with regard to the deviation caused by the discrete damage, the uniformly distributed damage yields a deviation more than twice as large as the other two damage scenarios.

In addition to the severity of the damage, its geometric position along the length of the beam plays an important role regarding the influence on the modal properties. Thereby, the influence of each geometric position additionally varies with regard to the eigenfrequency considered. An observation of Figures 7 and 8 reveals that, for instance, a damage position near the bearing (i.e., fishplate position 9) greatly affects the first eigenfrequency but has no noticeable effect on the second eigenfrequency. This is explained by the deflection shape: With the corresponding measured mode shapes in mind (cf. Figure 6), it is evident that a high eigenfrequency deviation occurs at the geometric positions where the corresponding mode shapes show a high curvature. Geometric positions with a low curvature - i.e., the geometric positions of the zero crossings - show a low deviation in the eigenfrequency extracted.

This observation emphasizes the well-known need for the inclusion of several eigenfrequencies in the objective function of the FE model updating procedure for the localization of all damaged fishplate positions along the length of the steel cantilever beam: The geometric position of the damage evidently possesses different effects on the different eigenfrequencies.

#### 4. Finite element model updating

As part of the vibration-based non-destructive damage assessment methods, the basic assumption of FE model updating is that damage-induced variations in the mechanical properties cause detectable changes in the structural dynamic behavior [32, 33]. Thus, in order to detect, locate and quantify damage, vibration measurement data is analyzed and damage features are extracted. In a second step, an FE model is updated to match the structural behavior observed. Most often, this is done in terms of stiffness deviations [34]. As hands-on trial and error approaches are time consuming and not feasible for complex engineering structures, the problem is formulated indirectly as an optimization problem [35, 15]. Thereby, the objective function compares the dynamic behavior of the numerical model to a target (i.e., damaged) state and an optimization algorithm is used to find a model to match this target state by modifying stiffness parameters of the respective parameterized FE model. As the excitation forces are not known for output-only measurement setups in civil engineering applications, the measured time domain data is of little use for FE model updating approaches. Thus, the objective function generally comprises the difference of modal parameters or transfer functions, extracted from the measured data using signal processing and modal analysis techniques.

A variety of applications of different FE model updating methods on numerical examples and experimental investigations has been conducted over the last years [3, 32, 33], pointing out and aiming to overcome several difficulties of model updating. Many issues arise due to two major sources of uncertainty affecting the model updating process.

One source of uncertainty is the measurement data itself, including further processing of the gathered data. Due to the inevitable spatial sparsity and noisiness of the measured data and also due to imperfections in the measurement equipment and setup, measured data is always a source of errors and uncertainty [36]. By careful planning of the measurement system and sensor setup, possible error sources might be discovered and removed. Considering incomplete and noisy measurement data, many attempts are made to generalize or regulate this source of uncertainty [37]. However, the fact remains that measurement uncertainty can merely be minimized, but never be fully eliminated. Even more uncertainty is introduced during the subsequent signal processing and extraction of modal characteristics of the physical structure [34]. Thereby, the outcome depends on the choice and application of the modal analysis technique [38]. This source of uncertainty can be addressed by applying uncertainty quantification. Examples for uncertainty quantification in model updating are probabilistic Bayesian approaches [39, 40, 41] and non-probabilistic fuzzy approaches [42, 43, 44]. However, in this work, FE

297 model updating is applied solely in the deterministic sense. Uncertainties due to measurement noise or further  
 298 signal processing is sought to be minimized by using a low-noise measurement setup (cf. Section 2.1) and an  
 299 advanced identification method for the extraction of modal data (cf. Section 3.1).

300 The second major source of possible uncertainties is the FE model used in the updating procedure. Mot-  
 301 tershead et al. [15] classified the sources of modelling uncertainties into reducible and irreducible by model  
 302 updating. By their definition, reducible sources are erroneous assumptions for model parameters, like material  
 303 or geometric properties. Thus, the correction of these properties is the aim of every model updating procedure.  
 304 Irreducible sources are discretization errors and idealization errors made, e.g., in the process of simplifying the  
 305 mechanical behaviour. The requirement derived from these assessments is that numerical models need to be  
 306 validated prior to their use for updating, so that at the end of the model updating process all three kinds of  
 307 modelling uncertainties are minimized. In this work, this recommendation is adapted by validating the FE  
 308 model prior to the model updating process. Thereby, the introduced FE model described in Section 2.3 was  
 309 examined and enhanced, e.g., regarding the consideration of the mass increase due to the wiring and sensors.  
 310 As oftentimes a constant systematic difference between the simulated modal quantities of the initial but vali-  
 311 dated FE model and the extracted modal quantities of the measurement remains, a formulation of a normalized  
 312 relative objective function is chosen in this work. This enables the mitigation of inherent constant systematic  
 313 errors between model and measurement.

314 Regarding the correction of the model parameters, a variety of different approaches exists [34]. Commonly,  
 315 design variables are mapped directly to structural properties such as stiffness values of individual finite elements.  
 316 If the defect location is unknown, this procedure usually entails a large amount of design variables, resulting  
 317 in an objective value space with many local minima [45]. Thus, many authors aim to keep the amount of  
 318 design variables as low as possible. A common example is to divide the numerical model into groups of FEs  
 319 and mapping one design variable per structural property of these formed FE groups [46, 47]. Another example  
 320 is to observe only a geometrically restricted area of the model, whereby, naturally, a prior assumption of the  
 321 defect location is required [48, 14]. Additionally, if the design variables are not constrained, the updating might  
 322 result in oscillatory stiffness values which can produce almost the same response as correct values, despite being  
 323 physically unrealistic [46, 49].

324 In order to address this problem, the application of a parameterized damage distribution function was  
 325 previously introduced by the authors [50, 51] and is utilized and extended in this work. The FE model updating  
 326 approach proposed using a damage distribution function is independent of the FE mesh resolution and of prior  
 327 assumptions about the defect location while only needing few design variables. By formulating the mapping of  
 328 the considered structural properties to the finite elements using a cumulative distribution function, a smooth,  
 329 realistic distribution is ensured. This forces the model updating process to focus on global structural dynamics  
 330 instead of over-fitting local deviations. As different damage scenarios like a cut or a stiffness degradation  
 331 have diverging effects on the stiffness properties of the structure, the method is extended by the possibility to  
 332 exchange different damage distribution functions. This offers the opportunity to imitate the damage behavior  
 333 and, with that, the damage scenario as good as possible. In addition, using different damage distribution  
 334 functions and a relative formulation of the objective function, many of the mentioned issues of common FE  
 335 model updating procedures are addressed. Thereby, the goal is to obtain a numerically efficient, well-posed  
 336 optimization problem, which can handle irreducible modelling errors. Other approaches, that are also motivated  
 337 by smoothly distributed structural properties and the reduction of the number of design variables, are analyzed  
 338 and successfully used in [11, 47, 52, 53]. Contrary to the approach proposed by the authors, these methods use  
 339 linear or quadratic functions to describe a so-called damage function. In addition, FEs are still grouped in these  
 340 approaches which is no longer necessary using the method subsequently presented in detail.

#### 341 4.1. Design variables

342 The formulation of the design variables strongly depends on the problem to be solved using model updating.  
 343 Since the aim of this work is damage localization along the length of the steel cantilever beam and damage  
 344 quantification, the parameterization should be able to identify the geometric location of the damage and its  
 345 intensity.

346 As no prior knowledge about the defect location is assumed for the procedure proposed, an updating of the  
 347 stiffness property of all  $n$  elements along the length of the numerical model is chosen by adapting the initial  
 348 Young's modulus  $E^0$  with a corresponding scaling factor  $\theta_i$

$$E_i^\theta = \theta_i \cdot E^0 \quad , \quad i \in [1, n]. \quad (4)$$

349 The modular setup of the presented damage assessment method is demonstrated by the use of two different  
 350 damage distribution functions, whereby their application to the three different damage scenarios is analyzed.

351 The possibility to use different damage distribution functions allows the best possible replication of the damage  
 352 scenario and a comparison between the results. In this work, a Gaussian and a continuous uniform damage  
 353 distribution function are considered.

354 Both distribution functions are defined along one control variable - the length of the beam  $L$  - and described  
 355 by the three design variables

$$\mathbf{x} = (\mu \ \sigma \ D)^T. \quad (5)$$

356 In the design variable vector  $\mathbf{x}$ ,  $\mu$  represents the geometrical position of the distribution function's center point  
 357 along the length,  $\sigma$  represents the width of the distribution and  $D$  represents the intensity of the damage. The  
 358 particular affiliations of the design variables corresponding to the two different damage distribution functions are  
 359 depicted in Figure 9 for the example design variable vector  $\mathbf{x} = (0.4 \text{ m} \ 0.1 \text{ m} \ 0.025)^T$ . Thereby, the definitions  
 360 of  $D$  and  $\mu$  are similar while the definition of  $\sigma$  varies slightly. Regarding the continuous uniform  
 361 function, 100% of the realizations correspond to  $\pm\sigma$ . Regarding the Gaussian distribution function, only 68.27%  
 362 of the realizations correspond to  $\pm\sigma$  and 95.45% correspond to  $\pm 2\sigma$ . This association represents the definition  
 363 of a standard Gaussian distribution function.

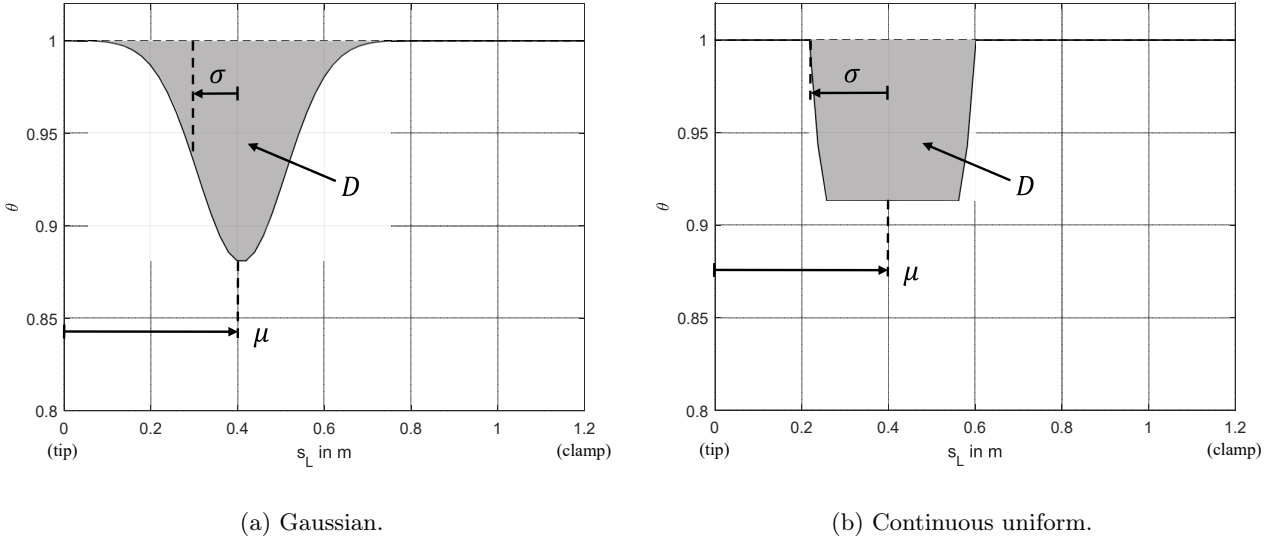


Figure 9: Affiliations of the three design variables demonstrated for the example design variable vector  $\mathbf{x} = (0.4 \text{ m} \ 0.1 \text{ m} \ 0.025)^T$  for the two damage distribution functions considered.

364 The damage intensity can be described as

$$D = \frac{1}{L} \int_L 1 - \theta(s_L) ds_L, \quad (6)$$

365 where  $L$  is the total length of the steel cantilever beam,  $s_L$  is the control variable along the beam length and  
 366  $\theta(s_L)$  is the stiffness scaling factor at position  $s_L$ . Relating this to the FE model, a stiffness scaling factor  $\theta_i$   
 367 is assigned to each element. Thus, the discrete damage intensity can be expressed as the sum over the total  
 368 number of elements along the length

$$D = \frac{1}{L} \sum_{i=1}^{N_L} (1 - \theta_i)(s_{L,i+1} - s_{L,i}). \quad (7)$$

369 Thereby, the term  $s_{L,i+1} - s_{L,i}$  is the actual length of every element. For the calculation of the stiffness  
 370 scaling factor  $\theta_i$  for each element, the respective cumulative distribution functions  $F(s_{L,i}|\mu, \sigma)$  of the damage  
 371 distribution functions considered are truncated to the interval  $0 \leq s_{L,i} \leq L$

$$\theta_i = 1 - DL \frac{F(s_{L,i+1}|\mu, \sigma, 0, L) - F(s_{L,i}|\mu, \sigma, 0, L)}{s_{L,i+1} - s_{L,i}}. \quad (8)$$

372 Figure 10 shows the distribution of the stiffness scaling factors  $\theta_i$  calculated for the same example design  
 373 variable vector and an example FE segmentation along the beam length. Additionally, the respective cumulative

374 distribution functions are displayed with values circled at each element position  $s_{L,i}$ .

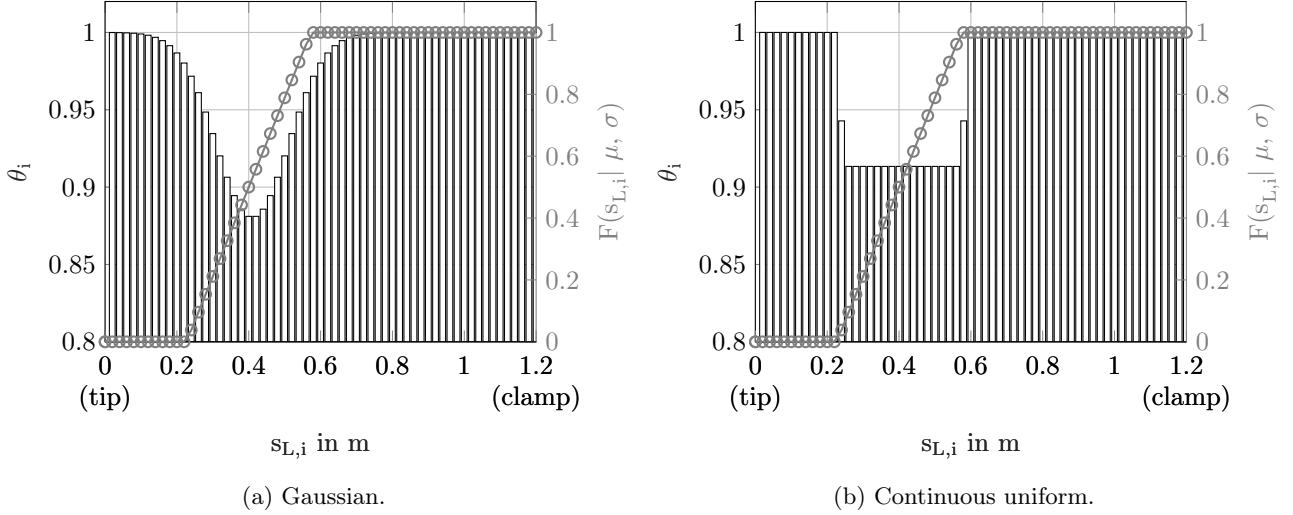


Figure 10: Distributions of the stiffness scaling factors  $\theta_i$  and the corresponding cumulative distribution function  $F(s_{L,i}|\mu, \sigma, 0, L)$  with values circled at each element positions  $s_{L,i}$  for the example design variable vector  $\mathbf{x} = (0.4 \text{ m } 0.1 \text{ m } 0.025)^T$ .

#### 375 4.2. Objective function

376 In this work, the FE model updating is based on eigenfrequencies, since these can be obtained experimentally  
 377 and under operational conditions in high quality. Only  $N_{\text{freqs}} = 4$  eigenfrequencies with a significant amplitude  
 378 in vertical direction are considered, as described in detail in Section 3. To evaluate the difference between the  
 379 relevant measured (i.e., target) and simulated eigenfrequencies, the root mean square error is utilized

$$\epsilon(\mathbf{x}) = \sqrt{\frac{1}{N_{\text{freqs}}} \sum_{k=1}^{N_{\text{freqs}}} \left( \frac{f_{\text{SD},k}(\mathbf{x}) - f_{\text{SR},k}}{f_{\text{SR},k}} - \frac{f_{\text{MD},k} - f_{\text{MR},k}}{f_{\text{MR},k}} \right)^2}. \quad (9)$$

380 In this equation, the eigenfrequencies  $f$  are denoted with a subscript  $(\cdot)_S$  for simulated and  $(\cdot)_M$  for measured  
 381 data. In addition, the subscript  $(\cdot)_D$  refers to the damaged state, while  $(\cdot)_R$  refers to the undamaged reference  
 382 state. Thereby, the design variable vector  $\mathbf{x}$  only influences the simulation results of the damaged states, while  
 383 all other terms of Equation 9 remain constant during the optimization run. With this relative formulation  
 384 of the objective function a constant initial error between the simulation and the measurement results in their  
 385 respective reference states can be taken into account.

386 As the value range of the stiffness scaling factors is not restricted to positive values by Equation 8, negative  
 387 values for  $\theta_i$  can arise for low values of  $\sigma$ , leading to meaningless FE results. To avoid this issue, all FE models  
 388 with negative stiffness values are rejected prior to the FE calculation. Since this approach creates a discontinuity  
 389 in the objective function, a constraint is added in order to facilitate the optimization process. Therefore, the  
 390 minimum stiffness scaling factor is used to formulate an inequality constraint which acts to restrict values below  
 391 15% of the original stiffness. This leads to the formulation of the bounded and constrained single-objective  
 392 optimization problem

$$\begin{aligned} &\text{minimise } \epsilon(\mathbf{x}) \\ &\text{s.t. } [0 \text{ m } 0 \text{ m } -0.1]^T \leq \mathbf{x} \leq [1.205 \text{ m } 0.2 \text{ m } 0.1]^T \\ &\text{s.t. } \min_i (\theta_i) > 0.15. \end{aligned} \quad (10)$$

393 The constraint is enforced using the exterior linear penalty method [54].

#### 394 4.3. Optimization scheme

395 The in-house object-oriented optimization framework EngiO [55] is utilized for the numerical optimization.  
 396 For the optimization procedure, the deterministic Global Pattern Search algorithm [56] is chosen, as this algo-  
 397 rithm was previously tested and performed well on various similar FE model updating procedures [51, 50]. The

398 connection between the optimization framework - written in Matlab programming syntax - and the FE calcula-  
 399 tions using Abaqus is also implemented using Matlab. Thereby, the input file of the FE model is adapted with  
 400 the new design variable vector of each optimization step as described in Section 4.1. Next, the FE calculation  
 401 is started and afterwards the result file containing the simulated eigenfrequencies is evaluated and the objective  
 402 function is calculated. Based on the result, a new design variable vector is provided by the optimization algo-  
 403 rithm and the procedure is repeated. In order to ensure comparability of the different optimization runs, the  
 404 maximum number of the objective function evaluations is set to 1500 for all data sets.

## 405 5. Results

406 As introduced in Section 3, the 1 h-measurements are divided into six 10 min-data sets each. This division  
 407 is also employed for the application of the FE model updating procedure. For each of the 27 damaged states  
 408 (i.e., 3 damage scenarios times 9 fishplate positions), six optimization runs are conducted. Therefore, the  
 409 eigenfrequencies used as input for the calculation of the objective function (cf.  $f_{MD,k}$  in Equation 9) are the  
 410 six 10 min-median values extracted from the considered 1 h-measurements. This results in  $27 \cdot 6$  optimization  
 411 results per damage distribution function applied. The eigenfrequencies of the reference state ( $f_{MR,k}$ ) used in  
 412 Equation 9 are the respective median values of all 1 h-measurements in the reference state listed in Table 6.

413 Before the optimal results are shown, two different example convergence behaviors are given using the Gaus-  
 414 sian distributed damage scenario of fishplate positions 1 (tip) and 9 (clamp). For these examples, the Gaussian  
 415 damage distribution function is employed. Figure 11 depicts the convergence behavior of the corresponding best  
 416 objective function values and Figures 12 and 13 show the convergence behavior of the three design variables for  
 417 the two damaged states considered.

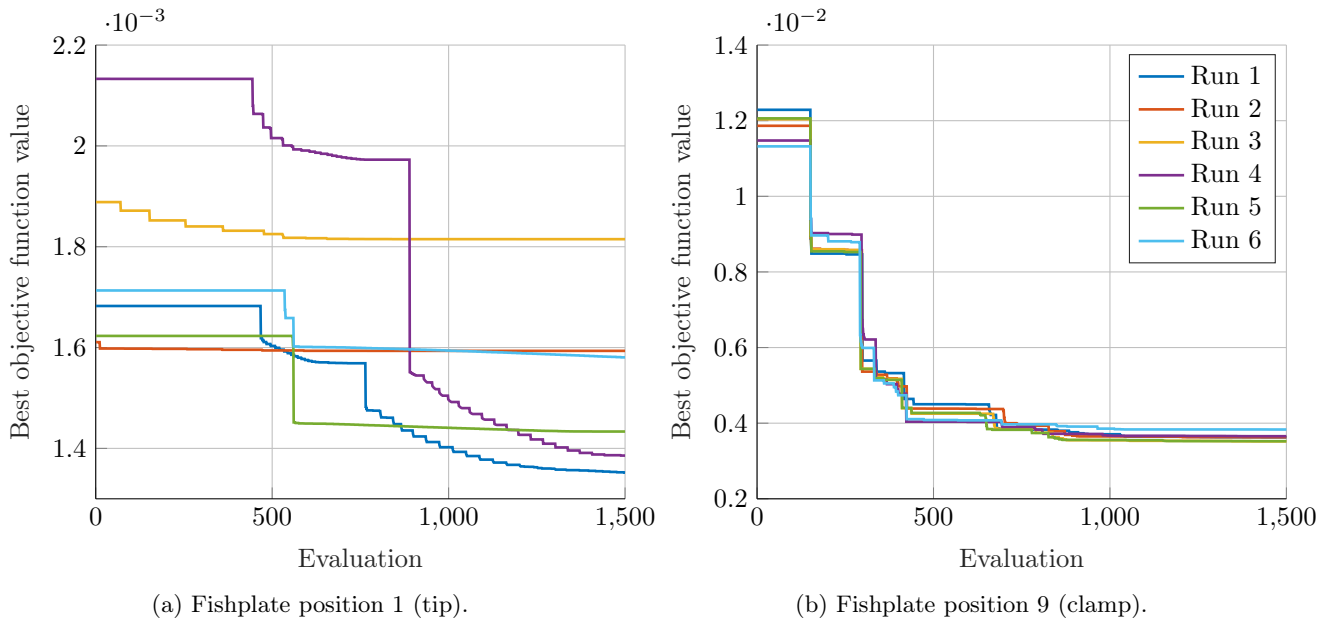


Figure 11: Convergence behavior of the best objective function value of the six optimization runs for the Gaussian distributed damage scenario of fishplate positions 1 and 9 using the Gaussian damage distribution function.

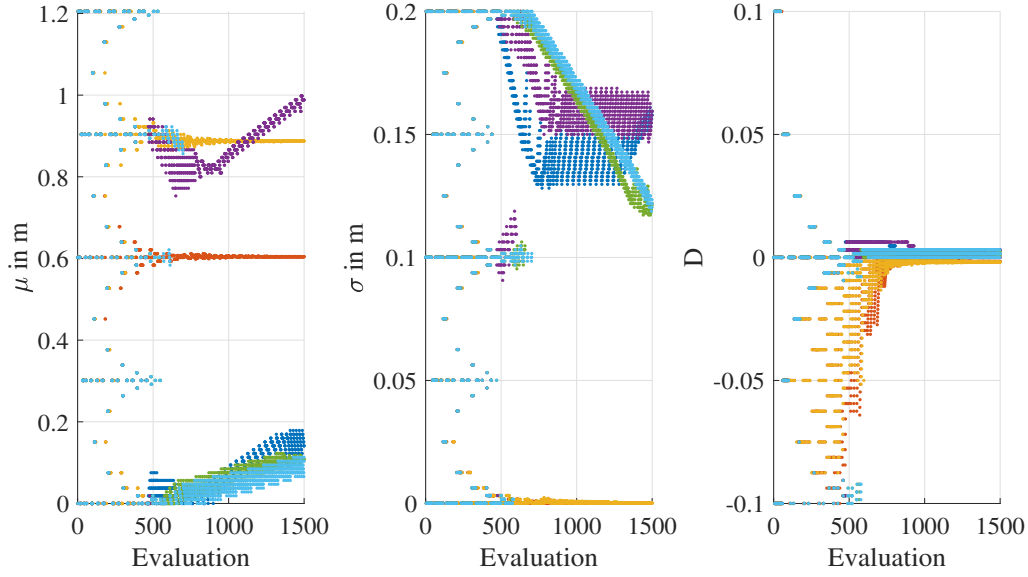


Figure 12: Convergence behavior of the three design variables of the six optimization runs for the Gaussian distributed damage scenario of fishplate position 1 (tip) using the Gaussian damage distribution function.

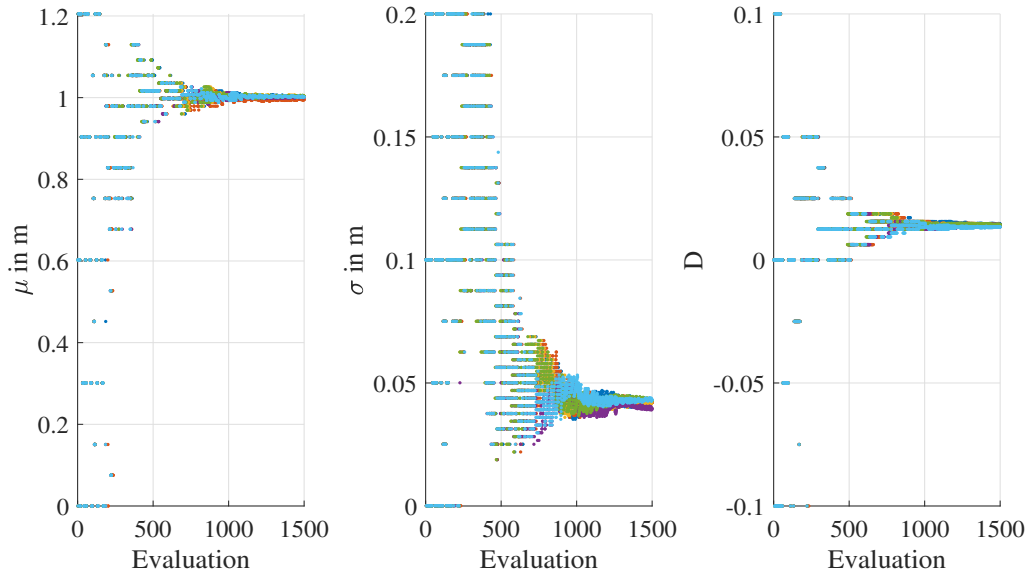


Figure 13: Convergence behavior of the three design variables of the six optimization runs for the Gaussian distributed damage scenario of fishplate position 9 (clamp) using the Gaussian damage distribution function.

418 Comparing the varying convergence behavior of the design variables and the best objective function value  
 419 for the two damaged fishplate positions, the influence of the geometric position of the damage along the length  
 420 of the steel cantilever beam is clearly visible. All six optimization runs regarding fishplate position 9 (clamp)  
 421 result in almost equivalent design variables and objective function values, presenting a conclusive localization  
 422 and quantification of this damage scenario. In contrast, the results concerning fishplate position 1 (tip) differ  
 423 partially significantly from each other. In Figure 12, the design variable  $\mu$ , for instance, converges in only  
 424 three of the six optimization runs towards the correct value of 0.075 m while values between 0.6 m and 1 m are  
 425 mistakenly found to be optimal in optimization runs 2 to 4. Additionally, the optimal values found for the  
 426 design variable  $\sigma$  vary within a range of 0.05 m, representing 25 % of the bounded space for this design variable.  
 427 Only the damage intensity converges to an equivalent value in all six optimization runs. However, this seemingly  
 428 optimal value is approximately 0, which is incorrect.



429 This inconclusive convergence behavior concerning the results for fishplate position 1 (tip) indicates a difficult  
 430 design variable space with multiple local minima. In comparison to the conclusive results regarding fishplate  
 431 position 9 (clamp), this reveals the difficulty to locate and quantify a damage at a geometric position very  
 432 close to the tip of the steel cantilever beam compared to the seemingly simple assessment of a damage near the  
 433 bearing. This conclusion matches the observations and thus the expectations from Section 3, where the modal  
 434 properties of the different damaged states were studied in detail. A damage positioned near the tip of the steel  
 435 cantilever beam has no significant influence on the stiffness properties and therefore on the structural behavior,  
 436 whereas a damage positioned near the bearing has a considerable effect. Thus, even adapting the stiffness of  
 437 all FEs along the beam length using a comparison of modal properties - as it is employed in the utilized and  
 438 in most other FE model updating procedures - is naturally limited by the effect a damage has on the (global)  
 439 stiffness properties and thus the global dynamic behavior of the structure considered.

440 To present the final results, the  $9 \cdot 3 \cdot 6$  optimal distributions of the stiffness scaling factor  $\theta$  resulting from the  
 441 respective optimal design variable vectors are displayed in Figures 14 and 15 for the two damage distribution  
 442 functions utilized. Thereby, one color is used per damage scenario as depicted in the legend.

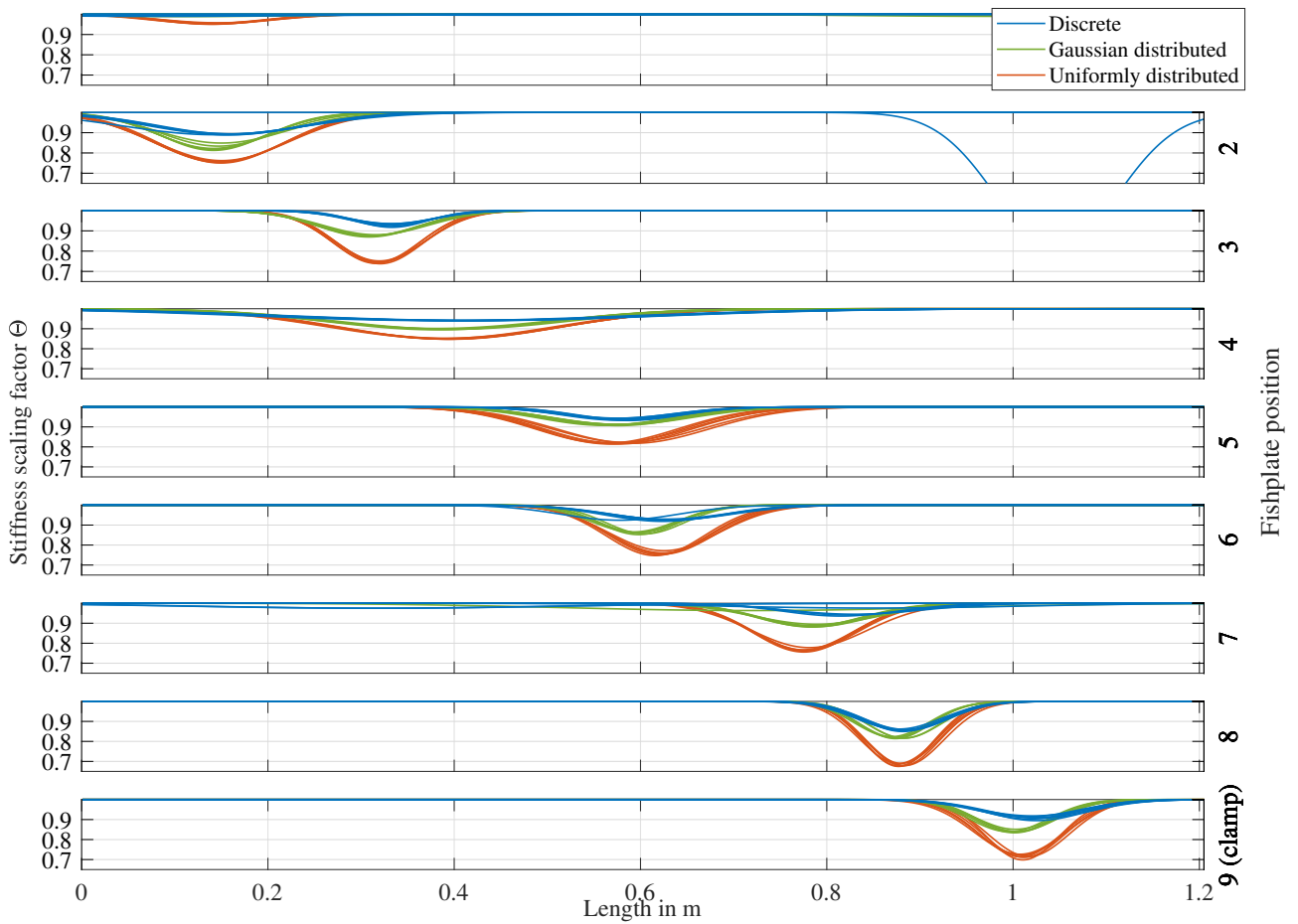


Figure 14:  $9 \cdot 3 \cdot 6$  optimal distributions of the stiffness scaling factor  $\theta$  for the nine fishplate positions and the three different damage scenarios for the Gaussian damage distribution functions.

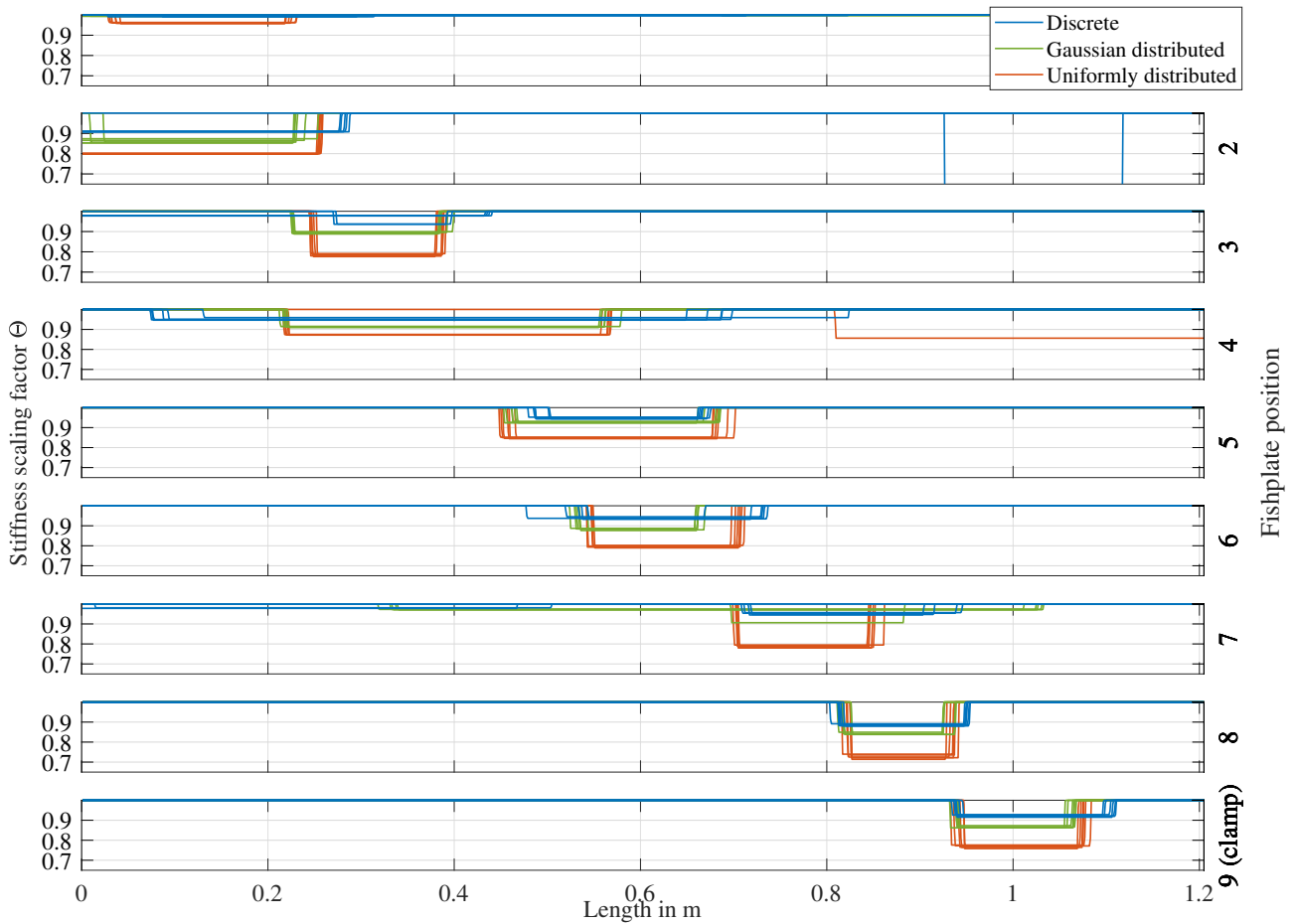


Figure 15: 9·3·6 optimal distributions of the stiffness scaling factor  $\theta$  for the nine fishplate positions and the three different damage scenarios for the continuous uniform damage distribution functions.

443 Overall, the results of the FE model updating procedure using only eigenfrequencies as the damage sensitive  
 444 feature demonstrate a conclusive localization of the nine different damage positions (i.e., fishplate positions)  
 445 and a distinct quantification between the three damage intensities employed. As already mentioned with regard  
 446 to Figures 11 to 13, the results for the damaged fishplate position 1 (tip) are especially inconclusive as this is  
 447 a position where damage has no significant effect on the global dynamic behavior of the steel cantilever beam.  
 448 Thus, the identification, localization and quantification of a defect at this particular position is very difficult  
 449 using the proposed or any other FE model updating procedure. Regarding the final results in Figures 14 and  
 450 15 for this position, only the fishplate with the most severe damage (i.e., the uniformly distributed damage)  
 451 is located correctly, whereas the other two damage scenarios are not found at all. This is the reason why the  
 452 results for fishplate position 1 at the tip of the steel cantilever beam are not included in the following detailed  
 453 discussion of the results.

454 Figure 16 allows for a precise observation of the results of the damage localization (i.e., design variable  $\mu$ )  
 455 for fishplate positions 2 to 9. The figure shows the difference between the optimal design variables obtained  
 456 using the FE model updating procedure and the actual measured (i.e., expected) values, depicted as dotted  
 457 black lines.

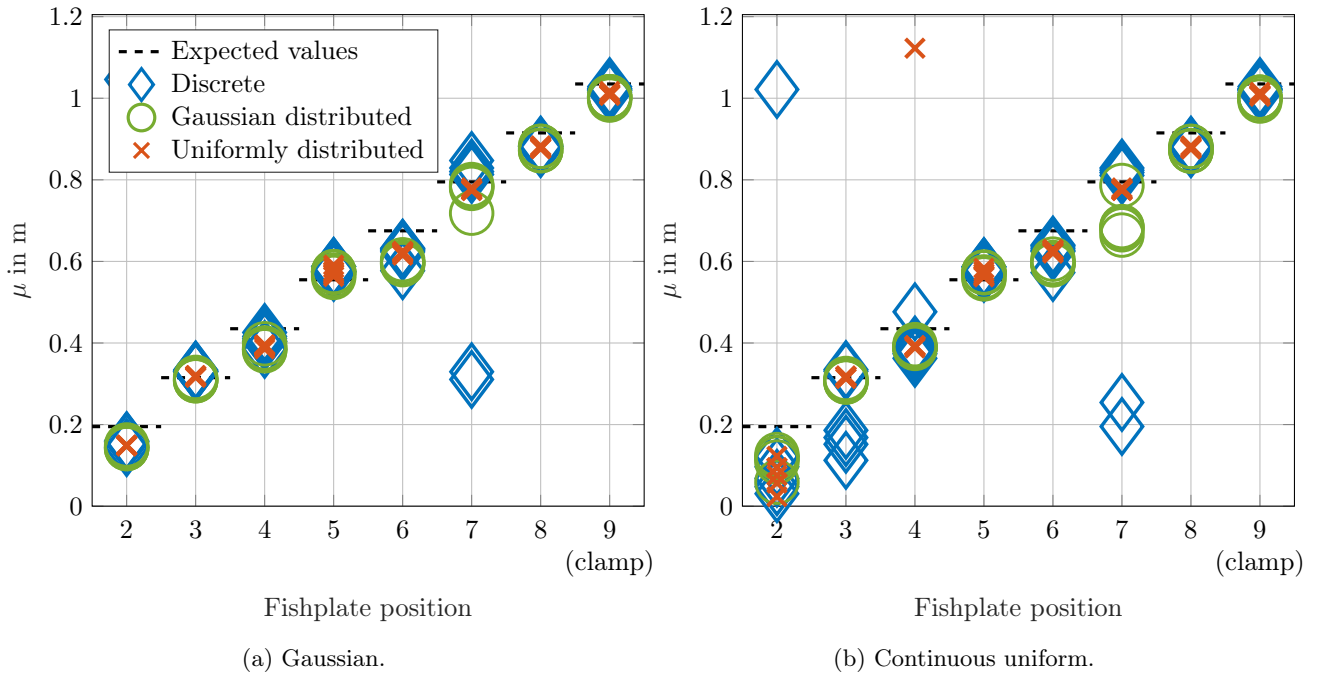


Figure 16: Comparison of the expected values to the optimal values obtained for the design variable  $\mu$  for each damage scenario of fishplate positions 2 to 9 using the two damage distribution functions considered.

458 The geometric positions of the discrete damage scenario (blue diamonds) are misidentified in some cases,  
 459 which is also visible in Figures 14 and 15. This observation unveils that, naturally, the localization of the discrete  
 460 damage scenario, having the least damage severity, is more difficult than the identification of the other two more  
 461 severe damage scenarios. In addition, the localization results using the Gaussian damage distribution function  
 462 (cf. Figure 16a) are slightly more consistent than the results using the continuous uniform damage distribution  
 463 function (cf. Figure 16b). Overall, however, it is evident that the employment of both damage distribution  
 464 functions yield accurate localization results, in most cases within  $\pm 0.05$  m of the expected geometric position of  
 465 the different damage scenarios. Thus, a successful localization of all fishplate positions considered is achieved.

466 The correct values expected for the design variable  $\sigma$  are equal for all fishplate positions per damage scenario  
 467 as the width of the damage is constant per damage scenario. Thereby, the width of the discrete damage is  
 468 0.001 m. The width of the Gaussian and the uniformly distributed damage is the same with a value of 0.093 m  
 469 ranging from the first to the last saw cut. Only the damage intensity differs for these two damage scenarios  
 470 due to the differing lengths of the saw cuts (cf. Figure 4). Figure 17 displays these expected values, depicted  
 471 as dotted lines in the color of the respective damage scenario, alongside the optimal values found for the design  
 472 variable  $\sigma$  obtained by the application of the two damage distribution functions considered. Because of the  
 473 definition of the design variable  $\sigma$  in the damage distribution functions (cf. Section 4.1 and Figure 9), the  
 474 optimal values for the design variable are multiplied by two so the expected values are compared to  $\pm\sigma$ .

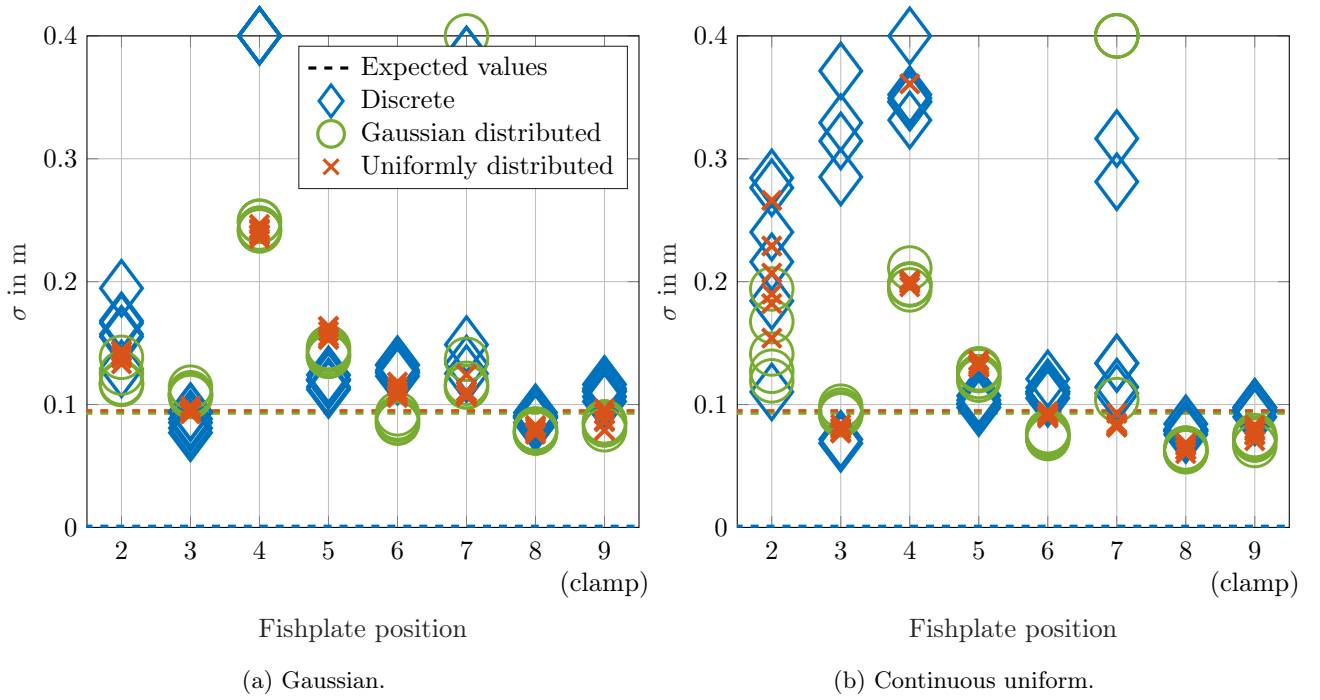


Figure 17: Comparison of the expected values to the optimal values obtained for the design variable  $\pm\sigma$  for each damage scenario of fishplate positions 2 to 9 using the two damage distribution functions considered.

475 Regarding the results for the Gaussian and the uniformly distributed damage scenarios (green circles and red  
 476 crosses), most of the optimal values obtained vary within a range of 0.06 m to 0.16 m. Only the values obtained  
 477 for fishplate positions 2 and 4 show more variation, which is again also visible in Figures 14 and 15. Thus, the  
 478 width of the two more severe damage scenarios is, in most cases, identified close to the actual width measured  
 479 to 0.093 m from the first to the last saw cut. This is why the identification of the damage width concerning the  
 480 Gaussian and the uniformly distributed damage scenario is considered to be successful. It is noticeable that the  
 481 width of the discrete damage (blue diamonds) is misidentified in all damage positions. As this damage scenario  
 482 represents a rupture of only 1 mm width in the fishplate specimen (cf. Figure 4), the results obtained for  $\sigma$   
 483 between 0.075 m and 0.2 m regarding this particular damage scenario are clearly incorrect. Again, this reveals  
 484 the difficulty to identify this least severe damage scenario correctly.

485 As with the design variable  $\sigma$ , the design variable  $D$  is also expected to be equal for all fishplate positions  
 486 per damage scenario as the intensity of the damage is also constant per damage scenario. For the calculation of  
 487 the expected values regarding the damage intensity, it is assumed that the alteration of the moment of inertia is  
 488 proportional to the alteration of the stiffness properties due to the different saw cuts into the fishplate specimens.  
 489 Hence, the stiffness scaling factor  $\theta_i$  in Equation 7 is exchanged with a scaling factor for the moment of inertia  
 490 of each finite element and the values for  $D$  are calculated for the three different damage scenarios, respectively.

491 The calculated values for  $D$  are 0.0005 for the discrete damage scenario, 0.0013 for the Gaussian distributed  
 492 damage scenario and 0.0024 for the uniformly distributed damage scenario. Compared to the optimal values  
 493 obtained using the FE model updating procedure, the analytically calculated values are off approximately by a  
 494 factor of ten. In the case of the Gaussian and uniformly distributed damage scenarios, this is due to the fact  
 495 that the calculation on the basis of the altered moment of inertia only considers six altered FEs as there are  
 496 six saw cuts in the respective fishplate specimens (cf. Figure 4). This rather underestimates the damage to  
 497 the structure as the impact on the stiffness properties is not locally limited to these six FEs. In contrast, the  
 498 damage distribution functions utilized in the FE model updating process are designed to identify a damaged  
 499 area. If the moment of inertia of all FEs between the first and last saw cut are scaled according to the induced  
 500 saw cuts, the values obtained for  $D$  are 0.021 for the Gaussian and 0.037 for the uniformly distributed damage  
 501 scenario. Hence, these values are similar to the optimal values obtained using the model updating procedure.  
 502 The optimal results for the damage intensity (i.e., design variable  $D$ ) are displayed in Figure 18. All results are  
 503 normalized to the results of the Gaussian distributed damage scenario. This enables a direct comparison of the  
 504 relative differences in  $D$  between the optimization-based solutions and the results for the analytical (moment  
 505 of inertia-based) calculations. The normalized analytical values for  $D$  (0.38 for the discrete, 1 for the Gaussian  
 506 distributed and 1.85 for the uniformly distributed damage scenario) are depicted as dotted lines in the color of

507 the respective damage scenario.

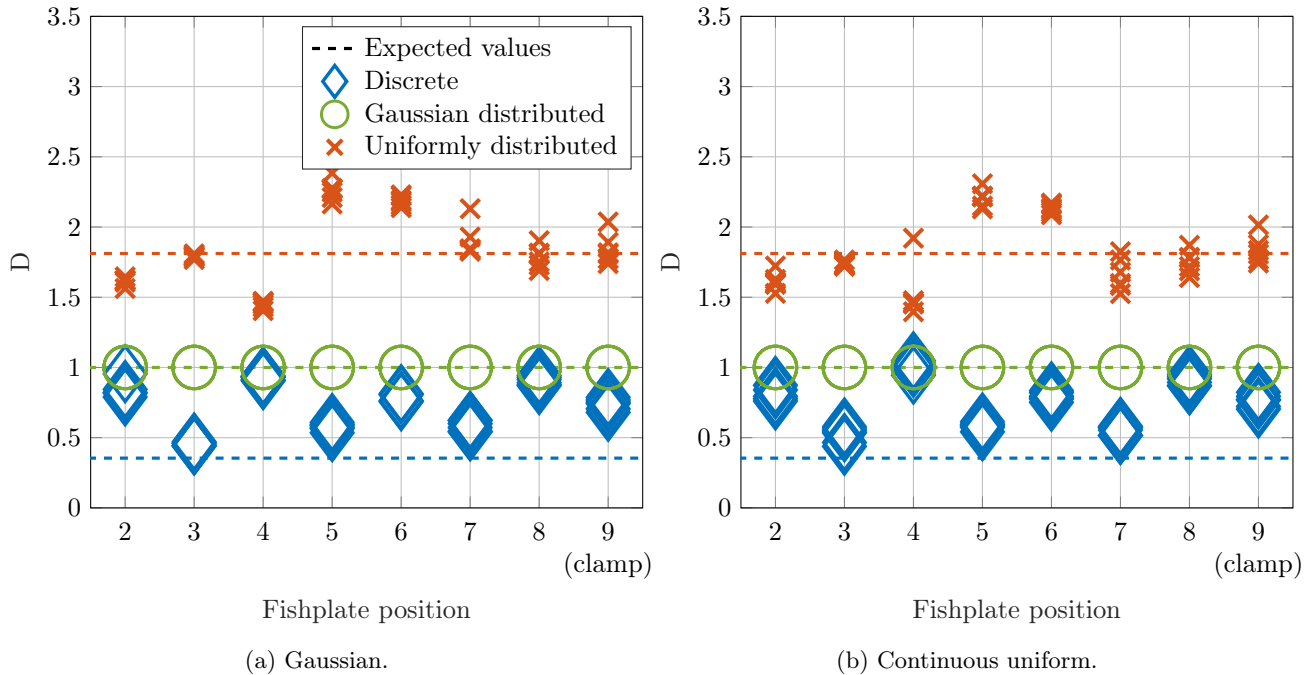


Figure 18: Comparison of the normalized analytical values to the optimal values obtained for the normalized design variable  $D$  for each damage scenario of fishplate positions 2 to 9 using the two damage distribution functions considered. All values are normalized to the results of the gaussian distributed damage scenario.

508 As expected, the optimal values obtained using the FE model updating procedure are fairly consistent  
 509 for each damage scenario. In addition, the increasing intensity of the three different damage scenarios is  
 510 distinctly visible for both damage distribution functions utilized as already discernible in Figures 14 and 15. The  
 511 percentage increase of the optimal results is close to the analytically calculated increase in damage severity. For  
 512 example, the normalized values for  $D$  are approximately by a factor of 1.85 higher for the uniformly distributed  
 513 compared to the Gaussian distributed damage for the analytical as well as the optimization-based results. Only  
 514 the damage intensity of the discrete damage scenario is slightly overestimated by the model updating procedure.  
 515 Altogether, also the quantification of the different damage severities introduced is considered successful. In  
 516 particular, it is possible to quantify the relative change in damage intensity which is, for example, relevant when  
 517 cracks are growing.

## 518 6. Conclusions and outlook

519 With this work, the laboratory experiment of a modular steel cantilever beam with the option to insert  
 520 different damage scenarios at different positions is presented in detail and the measurement data is made  
 521 available in open-access form. In addition, a systematic experimental validation of a deterministic FE model  
 522 updating procedure using four eigenfrequencies as damage sensitive features is demonstrated.

523 The results presented in Section 5 evidently show the successful precise localization of the nine different  
 524 damage positions within  $\pm 0.05$  m of the correct geometric positions along the 1.2 m-long beam. Also, the quan-  
 525 tification regarding the width and the intensity of the three different damage scenarios are found accurately.  
 526 The distinctive results emphasize the advantages of the parameterization chosen for the design variables within  
 527 the model updating process regarding robustness and applicability. In addition, the experimentally validated  
 528 formulation of the objective function using only eigenfrequencies enables the usage of a minimal sensor con-  
 529 cept for damage assessment. Furthermore, the demonstration of the experimental validation of the FE model  
 530 updating approach utilized reveals the applicability of the laboratory experiment presented for the validation  
 531 of SHM procedures addressing damage assessment. With the experimental setup enabling the opportunity to  
 532 introduce reversible damage scenarios of differing damage severities at a total of nine different damage positions,  
 533 a fundamental evaluation and comparison of different SHM methods is possible.

534 Looking more closely, naturally, some difficulties occurred and some observations are made regarding the  
 535 outlook of this work. The damage position at the tip of the steel cantilever beam was difficult to localize and

536 quantify correctly as a damage at this position has no significant influence on the stiffness properties and, thus,  
537 on the structural behavior of the steel cantilever beam. As a result, this particular damage scenario differs  
538 only marginally from the reference state, which results in a difficult design variable space, making it almost  
539 impossible for the optimization algorithm applied to find a correct solution. However, this finding represents a  
540 difficulty for all damage assessment methods based on modal parameters as they rely on the variation of the  
541 global structural behavior. In addition, the results of the discrete (i.e., the least intense) damage scenario show  
542 more variance with regard to the correct values than the other two more severe damage scenarios. Especially  
543 the width of this damage scenario is clearly overestimated. Further studies will include additional or different  
544 damage sensitive features potentially in a second objective function in order to analyze possible improvements  
545 enabled by multi-objective optimization.

546 Another interesting next step is the inclusion of the uncertainty regarding the modal properties. Therefore,  
547 the experiment is especially suited since the uncertainties are distinctly quantifiable in the laboratory experiment  
548 designed using the long 1h-measurements of the different damage scenarios and the respectively following  
549 repetitions of the measurements in reference state.

## 550 Data Availability Statement

551 The measurement data used in this work including a comprehensive documentation is published as an open-  
552 access data publication within the Research Data Repository of the Leibniz University Hanover that issues  
553 datasets with DOIs: <https://doi.org/10.25835/123gy6gm>.

## 554 Acknowledgments

555 We greatly acknowledge the financial support of the German Federal Ministry for Economic Affairs and  
556 Energy (research project *Multivariates Schadensmonitoring von Rotorblättern*, FKZ 0324157A) and Deutsche  
557 Bundesstiftung Umwelt (research project *Gebrauchstauglichkeit und Komfort von dynamisch beanspruchten*  
558 *Holztragwerken im urbanen mehrgeschossigen Hochbau*, AZ 34548/01-25) that enabled this work. In addition, we  
559 gratefully acknowledge the financial support of the Deutsche Forschungsgemeinschaft (DFG, German Research  
560 Foundation) - SFB-1463-434502799.

## 561 References

- 562 [1] J. Brownjohn, Structural health monitoring of civil infrastructure, *Philosophical Transactions of the Royal Society*  
563 *A: Mathematical, Physical and Engineering Sciences* 365 (1851) (2007) 589–622. doi:10.1098/rsta.2006.1925.
- 564 [2] O. Avci, O. Abdeljaber, S. Kiranyaz, M. Hussein, M. Gabbouj, D. J. Inman, A review of vibration-based damage  
565 detection in civil structures: From traditional methods to Machine Learning and Deep Learning applications,  
566 *Mechanical Systems and Signal Processing* 147 (2021) 107077. doi:10.1016/j.ymsp.2020.107077.
- 567 [3] S. W. Doebling, C. R. Farrar, M. B. Prime, A summary review of vibration-based damage identification methods,  
568 *The Shock and Vibration Digest* 30 (1998) 91–105.
- 569 [4] E. P. Carden, P. Fanning, Vibration based condition monitoring: A review, *Structural Health Monitoring* 3 (4)  
570 (2004) 355–377. doi:10.1177/1475921704047500.
- 571 [5] W. Fan, P. Qiao, Vibration-based Damage Identification Methods: A Review and Comparative Study, *Structural*  
572 *Health Monitoring* 10 (1) (2011) 83–111. doi:10.1177/1475921710365419.
- 573 [6] S. Das, P. Saha, S. K. Patro, Vibration-based damage detection techniques used for health monitoring of structures:  
574 a review, *Journal of Civil Structural Health Monitoring* 6 (3) (2016) 477–507. doi:10.1007/s13349-016-0168-5.
- 575 [7] K. Worden, C. R. Farrar, G. Manson, G. Park, The fundamental axioms of structural health monitoring, *Proceedings*  
576 *of the Royal Society A: Mathematical, Physical and Engineering Sciences* 463 (2082) (2007) 1639–1664. doi:  
577 10.1098/rspa.2007.1834.
- 578 [8] A. Rytter, *Vibrational Based Inspection of Civil Engineering Structures*, Vol. R9314, Dept. of Building Technology  
579 and Structural Engineering, Aalborg University, 1993.
- 580 [9] S. Doebling, C. Farrar, M. Prime, D. Shevitz, Damage identification and health monitoring of structural and  
581 mechanical systems from changes in their vibration characteristics: A literature review, Tech. Rep. LA-13070-MS,  
582 249299, Los Alamos National Lab. (LANL) (1996). doi:10.2172/249299.

- 583 [10] D. Sanders, Y. Kim, N. Stubbs, Nondestructive evaluation of damage in composite structures using modal param-  
584 eters, *Experimental Mechanics* (1992) 240–251.
- 585 [11] M. Abdel Wahab, G. De Roeck, B. Peeters, Parameterization of damage in reinforced concrete structures using  
586 model updating, *Journal of Sound and Vibration* 228 (4) (1999) 717–730. doi:10.1006/jsvi.1999.2448.
- 587 [12] F. D. Ju, M. E. Mimovich, Experimental diagnosis of fracture damage in structures by the modal frequency method,  
588 *Journal of Vibration and Acoustics* 110 (4) (1988) 456–463. doi:10.1115/1.3269550.
- 589 [13] E. Manoach, J. Warminski, L. Kloda, A. Teter, Numerical and experimental studies on vibration based methods  
590 for detection of damage in composite beams, *Composite Structures* 170 (2017) 26–39. doi:10.1016/j.compstruct.  
591 2017.03.005.
- 592 [14] K. Schröder, C. G. Gebhardt, R. Rolfes, A two-step approach to damage localization at supporting structures of  
593 offshore wind turbines, *Structural Health Monitoring* 17 (5) (2018) 1313–1330. doi:10.1177/1475921717741083.
- 594 [15] J. E. Mottershead, M. Link, M. I. Friswell, The sensitivity method in finite element model updating: A tutorial,  
595 *Mechanical Systems and Signal Processing* 25 (7) (2011) 2275–2296. doi:10.1016/j.ymsp.2010.10.012.
- 596 [16] R. Gorgin, Damage identification technique based on mode shape analysis of beam structures, *Structures* 27 (2020)  
597 2300–2308. doi:10.1016/j.istruc.2020.08.034.
- 598 [17] E. Figueiredo, E. Flynn, Three-story building structure to detect nonlinear effects, in: Report SHMTools data  
599 description, 2009.
- 600 [18] E. Figueiredo, G. Park, J. Figueiras, C. Farrar, K. Worden, Structural health monitoring algorithm comparisons  
601 using standard data sets (2009). doi:10.2172/961604.
- 602 [19] E. A. Johnson, H. F. Lam, L. S. Katafygiotis, J. L. Beck, A benchmark problem for structural health monitoring and  
603 damage detection, in: F. Casciati, G. Magonette (Eds.), *Structural Control for Civil and Infrastructure Engineering*,  
604 WORLD SCIENTIFIC, 2001, pp. 317–324. doi:10.1142/9789812811707\_0028.
- 605 [20] S. J. Dyke, D. Bernal, Beck, J. L. and Ventura, C., An experimental benchmark problem in structural health  
606 monitoring, *Proceedings of the Third International Workshop on Structural Health Monitoring*, Stanford, CA,  
607 USA.
- 608 [21] C. Krämer, C. De Smet, G. De Roeck, Z24 bridge damage detection tests, *Proceedings of the 17th International  
609 Modal Analysis Conference (IMAC)*, Kissimmee, Florida, USA (1999) 1023–1029.
- 610 [22] J. Maeck, G. De Roeck, Damage detection on a prestressed concrete bridge and rc beams using dynamic system iden-  
611 tification, *Key Engineering Materials* 167-168 (1999) 320–327. doi:10.4028/www.scientific.net/KEM.167-168.  
612 320.
- 613 [23] D. Tcherniak, G. C. Larsen, Application of oma to an operating wind turbine: now including vibration data from  
614 the blades, *Proceedings - 5th International Operational Modal Analysis Conference (IOMAC'13)*.
- 615 [24] D. Tcherniak, L. L. Mølgaard, Vibration-based shm system: Application to wind turbine blades, *Journal of Physics:  
616 Conference Series* 628 (2015) 012072. doi:10.1088/1742-6596/628/1/012072.
- 617 [25] T. Bull, M. D. Ulriksen, D. Tcherniak, The effect of environmental and operational variabilities on damage detection  
618 in wind turbine blades, *Proceedings of the 9th European Workshop on Structural Health Monitoring*, Manchester,  
619 UK.
- 620 [26] S. Wernitz, B. Hofmeister, C. Jonscher, T. Griebmann, R. Rolfes, A new open-database benchmark structure for  
621 vibration-based structural health monitoring, *Structural Control and Health Monitoring* n/a (n/a) (2022) e3077.  
622 doi:10.13140/RG.2.2.26051.48163.
- 623 [27] C. Hübler, B. Hofmeister, S. Wernitz, R. Rolfes, Validierung von daten- und modellbasierten methoden zur  
624 schadenslokalisierung, *Bautechnik* 99 (6) (2022) 433–440. doi:10.1002/bate.202200015.
- 625 [28] F. Levinzon, *Piezoelectric Accelerometers with Integral Electronics*, Springer International Publishing, Cham and  
626 s.l., 2015. doi:10.1007/978-3-319-08078-9.
- 627 [29] R. Brincker, L. Zhang, P. Andersen, Modal identification of output-only systems using frequency domain decompo-  
628 sition, *Smart Materials and Structures* 10 (3) (2001) 441–445. doi:10.1088/0964-1726/10/3/303.
- 629 [30] R. Brincker, C. Ventura, P. Andersen, Damping estimation by frequency domain decomposition, *Proceedings of  
630 the 19th International Modal Analysis Conference*, Kissimmee.

- 631 [31] R. J. Allemang, D. L. Brown, A correlation coefficient for modal vector analysis, in: Proceedings of the 1st interna-  
632 tional modal analysis conference, Vol. 1, SEM Orlando, 1982, pp. 110–116.
- 633 [32] J. E. Mottershead, M. I. Friswell, Model updating in structural dynamics: a survey, *Journal of Sound and Vibration*  
634 167 (2) (1993) 347–375. doi:10.1006/jsvi.1993.1340.
- 635 [33] E. Simoen, G. De Roeck, G. Lombaert, Dealing with uncertainty in model updating for damage assessment: A  
636 review, *Mechanical Systems and Signal Processing* 56-57 (2015) 123–149. doi:10.1016/j.ymsp.2014.11.001.
- 637 [34] M. I. Friswell, J. E. Mottershead, *Finite Element Model Updating in Structural Dynamics*, Vol. 38 of *Solid Mechanics*  
638 *and its Applications*, Springer Netherlands, 1995. doi:10.1007/978-94-015-8508-8.
- 639 [35] M. I. Friswell, Damage identification using inverse methods, *Philosophical Transactions of the Royal Society A:*  
640 *Mathematical, Physical and Engineering Sciences* 365 (1851) (2007) 393–410. doi:10.1098/rsta.2006.1930.
- 641 [36] M. Link, Updating of analytical models—review of numerical procedures and application aspects, in: *Proc., Struc-*  
642 *tural Dynamics Forum SD2000*, Research Studies Press, Baldock, UK, 1999, pp. 193–223.
- 643 [37] Z. Zhang, Y. Luo, Restoring method for missing data of spatial structural stress monitoring based on correlation,  
644 *Mechanical Systems and Signal Processing* 91 (2017) 266 – 277. doi:10.1016/j.ymsp.2017.01.018.
- 645 [38] E. Reynders, System Identification Methods for (Operational) Modal Analysis: Review and Comparison, *Archives*  
646 *of Computational Methods in Engineering* 19 (1) (2012) 51–124. doi:10.1007/s11831-012-9069-x.
- 647 [39] J. L. Beck, L. S. Katafygiotis, Updating Models and Their Uncertainties. I: Bayesian Statistical Framework, *Journal*  
648 *of Engineering Mechanics* 124 (4) (1998) 455–461. doi:10.1061/(ASCE)0733-9399(1998)124:4(455).
- 649 [40] L. S. Katafygiotis, K.-V. Yuen, Bayesian spectral density approach for modal updating using ambient data, *Earth-*  
650 *quake Engineering & Structural Dynamics* 30 (8) (2001) 1103–1123. doi:10.1002/eqe.53.
- 651 [41] C. Hizal, G. Turan, A two-stage bayesian algorithm for finite element model updating by using ambient response  
652 data from multiple measurement setups, *Journal of Sound and Vibration* 469 (2020) 115139. doi:10.1016/j.jsv.  
653 2019.115139.
- 654 [42] M. Savoia, Structural reliability analysis through fuzzy number approach, with application to stability, *Computers*  
655 *& Structures* 80 (12) (2002) 1087–1102. doi:10.1016/S0045-7949(02)00068-8.
- 656 [43] T. Haag, J. Herrmann, M. Hanss, Identification procedure for epistemic uncertainties using inverse fuzzy arithmetic,  
657 *Mechanical Systems and Signal Processing* 24 (7) (2010) 2021–2034. doi:10.1016/j.ymsp.2010.05.010.
- 658 [44] T. Haag, S. Carvajal González, M. Hanss, Model validation and selection based on inverse fuzzy arithmetic, *Me-*  
659 *chanical Systems and Signal Processing* 32 (2012) 116–134. doi:10.1016/j.ymsp.2011.09.028.
- 660 [45] M. Bruns, B. Hofmeister, D. Pache, R. Rolfes, Finite element model updating of a wind turbine blade—a comparative  
661 study, in: *EngOpt 2018 Proceedings of the 6th International Conference on Engineering Optimization*, Springer  
662 International Publishing, 2019, pp. 569–580. doi:10.1007/978-3-319-97773-7\_51.
- 663 [46] R. Levin, N. Lieven, Dynamic finite element model updating using simulated annealing and genetic algorithms,  
664 *Mechanical Systems and Signal Processing* 12 (1) (1998) 91–120. doi:10.1006/mssp.1996.0136.
- 665 [47] A. Teughels, J. Maeck, G. De Roeck, Damage assessment by FE model updating using damage functions, *Computers*  
666 *& Structures* 80 (25) (2002) 1869–1879. doi:10.1016/S0045-7949(02)00217-1.
- 667 [48] G.-H. Kim, Y.-S. Park, An improved updating parameter selection method and finite element model update using  
668 multiobjective optimisation technique, *Mechanical Systems and Signal Processing* 18 (1) (2004) 59–78. doi:10.  
669 1016/S0888-3270(03)00042-6.
- 670 [49] A. J. García-Palencia, E. Santini-Bell, A Two-Step Model Updating Algorithm for Parameter Identification of  
671 Linear Elastic Damped Structures, *Computer-Aided Civil and Infrastructure Engineering* 28 (2013) 509–521. doi:  
672 10.1111/mice.12012.
- 673 [50] M. Bruns, B. Hofmeister, C. Hübler, R. Rolfes, Damage localization via model updating using a damage distribution  
674 function, in: *Structural Health Monitoring 2019*, DEStech Publications, Inc, Lancaster, PA, 2019. doi:10.12783/  
675 shm2019/32202.
- 676 [51] M. Bruns, B. Hofmeister, T. Griefmann, R. Rolfes, Comparative study of parameterizations for damage localiza-  
677 tion with finite element model updating, in: *Proceedings of the 29th European Safety and Reliability Conference*  
678 *(ESREL)*, Research Publishing Services, Singapore, 2019. doi:10.3850/978-981-11-2724-3\_0713-cd.



- 679 [52] A. Teughels, G. De Roeck, J. A. Suykens, Global optimization by coupled local minimizers and its application to  
680 FE model updating, *Computers & Structures* 81 (24-25) (2003) 2337–2351. doi:10.1016/S0045-7949(03)00313-4.
- 681 [53] S. Schommer, V. H. Nguyen, S. Maas, A. Zürbes, Model updating for structural health monitoring using static and  
682 dynamic measurements, *Procedia Engineering* 199 (2017) 2146–2153. doi:10.1016/j.proeng.2017.09.156.
- 683 [54] C. A. Coello Coello, Theoretical and numerical constraint-handling techniques used with evolutionary algorithms:  
684 a survey of the state of the art, *Computer Methods in Applied Mechanics and Engineering* 191 (11) (2002) 1245 –  
685 1287. doi:10.1016/S0045-7825(01)00323-1.
- 686 [55] R. Berger, M. Bruns, A. Ehrmann, A. Haldar, J. Häfele, B. Hofmeister, C. Hübler, R. Rolfes, Engio – object-  
687 oriented framework for engineering optimization, *Advances in Engineering Software* 153 (2021) 102959. doi:10.  
688 1016/j.advengsoft.2020.102959.
- 689 [56] B. Hofmeister, M. Bruns, R. Rolfes, Finite element model updating using deterministic optimisation: A global  
690 pattern search approach, *Engineering Structures* 195 (2019) 373 – 381. doi:10.1016/j.engstruct.2019.05.047.